ANALYSIS OF UPWELLING CHANGES IN THE EASTERN EQUATORIAL PACIFIC DURING EL NIÑO SOUTHERN OSCILLATION

A Thesis

by

CARLOS FERNANDO PERUGACHI SALAMEA

Submitted to the Office of Graduate Studies of
Texas A&M University
in partial fulfillment of the requirements for the degree of

MASTER OF SCIENCE

December 2011

Major Subject: Oceanography

ANALYSIS OF UPWELLING CHANGES IN THE EASTERN EQUATORIAL PACIFIC DURING EL NIÑO SOUTHERN OSCILLATION

A Thesis

by

CARLOS FERNANDO PERUGACHI SALAMEA

Submitted to the Office of Graduate Studies of
Texas A&M University
in partial fulfillment of the requirements for the degree of

MASTER OF SCIENCE

Approved by:

Chair of Committee,	Benjamin Giese
Committee Members,	Gerald North
	Howard Seidel
Head of Department,	Piers Chapman

December 2011

Major Subject: Oceanography

ABSTRACT

Analysis of Upwelling Changes in the Eastern Equatorial Pacific

during El Niño Southern Oscillation. (December 2011)

Carlos Fernando Perugachi Salamea, B.S., America Technological University

Chair of Advisory Committee: Dr. Benjamin Giese

The ocean reanalysis Simple Ocean Data Assimilation (SODA) 2.2.4 is used to explore the changes in upwelling from normal conditions to either El Niño or La Niña conditions. Physical and thermodynamic variables from the reanalysis are used to explore the structure and behaviour of El Niño Southern Oscillation (ENSO) events. The results of this analysis show that sea surface temperature (SST), entrainment velocity, wind stress, mixed layer depth, wind curl, and heat content anomalies are in general agreement with ENSO theory. Interestingly, the distribution of upwelling based on the entrainment velocity is very patchy, which led us to explore zonal and meridional sections of vertical velocity. We used three methods to compute changes in upwelling during ENSO events. The first method computes upwelling within the areas of SST anomalies during ENSO events. During El Niño events upwelling shows prominent decadal variability, while during La Niña the decadal variability is weaker. A new upwelling index is used for the second method, and upwelling is computed in the areas of strong upwelling anomalies. The variability of upwelling is higher in periods of reduced upwelling than in periods of strong upwelling. Despite the fact that the new

index is computed independently, it agrees in the timing of the index used to define ENSO events for this research. The first and second methods show that the amplitude of SST anomalies and upwelling anomalies do not have a direct relationship, suggesting that upwelling does not explain all of the variance in SST. The last method used is to compute changes in upwelling in the Niño 1+2 region during ENSO events. In the east Pacific there is almost no correlation between upwelling and SST anomalies during ENSO, but this might be attributed to the fact that the Niño 1+2 region is a relatively small region compared to the Niño 3.4 region that is used to define ENSO events. In general, the time series of SST and upwelling anomalies agree well just in the cases when ENSO events are prominently in the eastern Pacific. A comparison between yearly fisheries data from Ecuador and Peru and monthly data of SST anomalies during ENSO years is presented showing that during El Niño events the fish catch decreases and during La Niña events the fish catch increases. We infer that the increase or decrease in fish catch is associated to changes in fish populations, and that these changes are mainly due to availability of nutrients and changes in temperature during ENSO events.

DEDICATION

I dedicate my job to my family. To my parents Carlos and Lucía for their continue support and love in every moment in my life. To my brother Xavier and my sister Wendy, for being with me unconditionally. To the memory of my brother Diego, who is always in my mind, and in my heart. And to the woman who inspired me every day, giving happiness and love into my life, Paola.

This thesis is dedicated to all of you

NOMENCLATURE

20CRv2	20th Century Atmospheric Reanalysis Version 2
CHI	Center of Heat Index
CUI	Center of Upwelling Index
DJF	December-January-February
ENSO	El Niño Southern Oscillation
FAO	Food and Agriculture Organization of the United Nations
GDP	Gross Domestic Product
HC	Heat Content
ICOADS	International Comprehensive Ocean-Atmosphere Data Set
IMARPE	Instituto del Mar del Peru
INP	Instituto Nacional de Pesca del Ecuador
KPP	K-profile Parameterization
MBT	Mechanical Bathythermograph
MLDR	Mixed Layer Depth
NDJ	November-December-January
NOAA	National Oceanic and Atmospheric Administration
POP	Parallel Ocean Model
SLP	Sea Level Pressure
SO	Southern Oscillation
SODA	Simple Ocean Data Assimilation

SST	Sea Surface Temperature
TOGA	Tropical Ocean-Global Atmosphere Program
TAU	Wind Stress
W	Vertical Velocity
WCURL	Wind Stress Curl
WE	Entrainment Velocity
WOD09	World Ocean Database 2009
XBT	Expandable Bathythermograph

TABLE OF CONTENTS

Page

LIST OF FIGURES

FIGURE Page

FIGURE Page

CHAPTER I

INTRODUCTION AND

LITERATURE REVIEW

A. History of ENSO

El Niño Southern Oscillation (ENSO) is an ocean-atmosphere phenomenon, and it is considered part of the most important energetic global anomalies in the Earth's climate. This phenomenon was called El Niño by Peruvian fishermen in the nineteenth century, who described El Niño as the warm ocean current that flows along the west coast of South America around Christmas time. In recognition of this timing they called this phenomenon El Niño referring to the Christ child in Spanish [*Cane*, 2005; *Philander*, 1990]. Early studies carried out by geographers concluded that the warm conditions in some years was stronger than in others, and that sometimes these conditions were accompanied with oceanic and climatic phenomena [*Wang and Fiedler*, 2006]. The name El Niño came to be used for the interannual phenomena replacing annual occurrence [*Wang and Fiedler*, 2006].

This thesis follows the style of *Journal of Geophysical Research*.

B. ENSO mechanisms

1. Physical processes triggering ENSO phenomena

Sir Gilbert Walker was motivated by the occasional disastrous failures of the Indian monsoon to study El Niño. In the 1920s and 1930s, he found that between the western and eastern Pacific Ocean there is a difference in atmospheric surface pressure, associated with the warm ocean surface region over the western Pacific, and the cold region over the eastern Pacific. The difference in sea level pressure (SLP) is called Southern Oscillation (SO) [*Walker*, 1923,1924;*Walker and Bliss*, 1932].

The meteorologist Jacob Bjerknes in 1969 suggested that El Niño and the Southern Oscillation are part of the same phenomenon. These two processes were later called the El Niño Southern Oscillation (ENSO) phenomenon [*Wang and Picaut*, 2004]. Furthermore, Bjerknes stated that warming observed in the central and eastern Pacific is derived from a feedback process between the ocean and atmosphere [*Wang and Picaut*, 2004; *Wang and Fiedler*, 2006]. One important aspect of the Bjerknes hypothesis is that positive ocean-atmosphere feedback describes how normal conditions in the central and eastern Pacific change to a warming sea surface temperatures and a decrease in the trade winds [*Philander*, 1990; *Wang and Picaut*, 2004; *Wang and Fiedler*, 2006]. However, this positive feedback mechanism would cause a permanent warm state in the Pacific Ocean, and what causes the shift between the air-sea interaction by that time was not clear.

In the 1980s the Tropical Ocean-Global Atmosphere (TOGA) program was established in order to have a better understanding and prediction of ENSO. After 1980,

four major negative feedbacks were proposed to explain the shift between a warm ocean state to a cold phase denominated by La Niña [*Philander*, 1990]. These negative feedbacks are: wave reflection at the western boundary or delayed oscillator [*Suarez and Schopf*, 1988; *Battisti and Hirst*, 1989], a recharge-discharge process or recharge oscillator [*Jin*, 1997], a western Pacific wind-forced Kelvin wave or western Pacific oscillator [*Weisberg and Wang*, 1997; *Wang et al*.,1999], and anomalous zonal advection the advective-reflective oscillator [*Picaut et al*., 1997]. It is expected that more than one of these oscillators may operate in nature and it has been suggested that a unified oscillator or multi mechanism system exits [*Wang* 2001; *Wang and Picaut*, 2004].

C. Physical and biological consequences of ENSO

The effects of ENSO are global, however in extratropical latitudes the effects are not as strong as in the tropical Pacific Ocean and in the contiguous continents [*Sarachik and Cane,* 2010]. Among some of the physical effects caused by ENSO during its warm phase are: an increase in rainfall in countries such Ecuador and Peru, and drought in Indonesia. Other effects associated with ENSO are: A change of the Indian monsoon, changes in rainfall in the western Pacific, changes in temperature in the tropical atmosphere, and suppression of hurricanes in the Atlantic [*Giese et al*., 2010; *Sarachik and Cane,* 2010]. Variations of SST observed during the phases of ENSO cause different impacts in the biology of marine species that inhabit the tropical Pacific Ocean. SST changes also imply different patterns of migration for marine species due to the cold or warm states. In addition, changes in upwelling cause important changes in primary production affecting not only patterns of migration but also the correct

development of species in terms of size and fitness that may affect the fish populations. Upwelling is the main process that transports nutrients from the deep ocean where the primary production is not possible due to a lack of light, to the euphotic zone where primary production is carried out because of suitable conditions for photosynthesis.

Primary production is the first trophic level of the food web or food chain, and for this process two principal conditions are necessary. These conditions are the availability of nutrients and light. Other factors play a significant role in primary production, such as availability of iron, but are less important than the two first described. Hence changes in upwelling cause changes in the availability of nutrients for primary production. If the primary production is reduced, then the amount of biomass in the higher trophic levels decreases, and thus the abundance of fish available to the fishery industry is impacted.

D. Economical and social impacts of ENSO

ENSO impacts affect a large part of the globe. Depending on the phase of ENSO (warm or cold), the areas affected can be dry or wet in terms of precipitation, and warm or cool in terms of sea surface temperature. Countries that are affected include Australia, Brazil, Ecuador, Peru, Bolivia, and Indonesia. These impacts cause important economical, social, and environmental consequences in the regions affected by ENSO phenomenon. Additionally an increase in rainfall due to ENSO causes economical impacts because of the flooding.

Depending on how big the changes in primary production are due to changes in upwelling, the upper trophic levels may be affected, and may cause enormous economic impact for countries such Ecuador in which the economic income generated by the

fishery is about 6.3% (year 1998) of Gross Domestic Product (GDP) [*Food and Agriculture Organization of the United Nations*, FAO]. Even though Ecuador is a relatively small country in terms of land area (approximately 256,370 km²) its territorial seas cover a significant maritime area (1,060,053 km²); hence the impacts on fisheries in the economy of the country are significant.

The main goal of this research is to determine and assess changes in upwelling in the eastern equatorial Pacific Ocean as a consequence of ENSO, specifically in the equatorial coastal areas. In this research we focus on the consequences in the oceanic area off the coast of Ecuador (Niño regions 1+2, 3), and the response of the eastern equatorial Pacific in terms of upwelling.

CHAPTER II

DATA AND METHODS

A. SODA methodology

1. POP Ocean Model

For this study we rely on data obtained from the Simple Ocean Data Assimilation (SODA) [*Carton and Giese*, 2008] to explore the changes in upwelling in the tropical Pacific during ENSO years. The reanalysis uses the Parallel Ocean Model (POP) [*Smith et al*., 1992], which has a resolution of 0.25° x 0.4° x 40 vertical levels, and SODA software. To compute mixing the ocean model uses a vertical K-profile parameterization (KPP), whereas the lateral is resolved using biharmonic mixing [*Carton and Giese*, 2008].

The ocean circulation model is forced using the 20th Century Reanalysis version 2 (20CRv2) atmospheric data set [*Whitaker et al*., 2004; *Compo et al*., 2006; *Compo et al*., 2008]. The ocean model uses wind stress from the atmospheric reanalysis for the surface momentum fluxes. To compute heat and freshwater fluxes the ocean model uses data from 20CRv2.

The atmospheric reanalysis uses surface observations and an Ensemble Kalman Filter data assimilation methodology [*Whitaker and Hamill*, 2002, *Whitaker et al.*, 2004; *Anderson et al.*, 2005; *Compo et al.*, 2006].

2. SODA 2.2.4 software

The assimilation of temperature and salinity observations is carried out every 10 days. Corrections are introduced at every time step, and the incremental corrections are calculated following the methodology presented by *Bloom et al.* [1996]. Average fields of the output temperature, salinity and velocity are saved every 5 days, and are then remapped onto a horizontal grid of 0.5°x0.5° [*Jones*, 1999].

The World Ocean Database 2009 (WOD09) data is used to obtain the temperature and salinity profiles [*Boyer et al*., 2009], and SST data is obtained from the International Comprehensive Ocean-Atmosphere Data Set (ICOADS 2.5). A fall-rate correction has been applied to the expandable bathythermograph (XBT) and the mechanical bathythermograph (MBT), in order to correct the bias errors introduced by these instruments in the observations used in SODA [*Levitus et al.,* 2009].

CHAPTER III

ANALYSIS

A. Objectives

The objectives of this study are:

Determine and assess the changes in upwelling in the eastern equatorial Pacific Ocean as a consequence of ENSO, in the oceanic area off the coast of Ecuador (El Niño regions 1+2, 3).

Verify the impacts of ENSO in this region in terms of upwelling, which in turn impact the populations of fish, and consequently the fishery industry and the economy.

Determine a way to obtain a correlation between the Center of Heat Index (CHI) and upwelling that allows to us verify that the values for CHI are higher for El Niño events when upwelling is minimum, and that CHI has lower values for la Niña years when upwelling is maximum.

Analyze fisheries data for the eastern equatorial Pacific Ocean, specifically for the coast off of Ecuador and Peru that correspond to the Niño 1+2 region, and contrast it with changes in upwelling and downwelling in order to assess the impacts of El Niño and La Niña.

B. Physical and thermodynamic properties in SODA 2.2.4 during ENSO years

1. The CHI index

The SODA 2.2.4 ocean reanalysis is used to explore changes in upwelling from normal conditions to either El Niño or La Niña conditions. The SST (Sea Surface

Temperature) data from SODA 2.2.4 is used to describe change in El Niño events. In the reanalysis SST anomalies are stronger than in SST reconstructions particularly from 1871-1920. For this research El Niño and La Niña events are defined according to the new index Center of Heat Index (CHI) proposed by *Giese and Ray* [2011]. CHI is an index that describe the amplitude, the longitude, and the area over which El Niño occurs. Other indexes such as Niño 3.4 SST used to define ENSO by the National Oceanic and Atmospheric Administration (NOAA), are fixed in space and so when the structure of ENSO changes, it can be an ambiguos index for measuring El Niño. The CHI exists if the SST anomaly is greater than 0.5 °C for 5 consecutive months over an area greater than the Niño 3.4 region, within a band of the tropical Pacific between 5°N and 5°S and between 120°E-70°W.

The same criteria is applied to define La Niña, with the difference that the temperature anomaly must be less than -0.5 °C. We defined El Niño and La Niña years using the list of El Niño and La Niña years based on CHI amplitude presented by *Giese and Ray* [2011].

2. Definition of strong El Niño and La Niña years according to CHI

Since the maximum values of CHI amplitude occur in the months December-January-February (DJF), the criteria applied to define El Niño years here is: if the DJF CHI Amplitude is greater than or equal to 1 the year is defined as a strong El Niño year. For La Niña most of the lowest values of CHI amplitude occurs in November-December-January (NDJ), so the criteria for this case is when NDJ CHI amplitude is lower than or equal to -1, the year is defined as a strong La Niña year. Using this criteria

to determine strong El Niño and La Niña events, there are a total of 24 El Niño events, and 29 La Niña events for the period 1871-2008.

3. Procedure to obtain the anomaly for each variable analyzed

For every variable analyzed from the data set we removed the 11-year climatology in order to obtain the corresponding anomalies. We use this procedure since the period of time that is covered for the data is long, and if we calculate the climatology over the entire record, there will be prominent trends or variability [*Giese and Ray*, 2011]. The 11-year climatology is calculated as a function of time in which we keep the low frequency component. The 11-year climatology is calculated using an eleven-year window. Since the data set covers the period 1871-2008, we separated the first 5 years 1871-1875, the 5 last years 2004-2008, and the years in the middle of these periods 1876-2003. We use a constant climatology that covers the 11 first years for the period between 1871 and 1875. For the last period (2004-2008), a constant climatology is calculated as well, using for this case the last 11 years of the record. To compute the climatology for the years from 1876 to 2003 we use an eleven-year moving window climatology [*Giese and Ray*, 2011]. Finally the climatology was subtracted from the original variable to obtain the anomaly.

4. Procedure to obtain the composite figure for the variables analyzed

Composite figures were calculated by averaging the anomalies for each variable for strong El Niño or La Niña years. Using the definition presented in the section 2, results in an average of 24 El Niño events, and 29 for La Niña events.

5. Exploring the variables in SODA

We begin by showing SST, wind stress (TAU), entrainment velocity (WE), vertical velocity (W), mixed layer depth (MLDR), wind stress curl (WCURL), and heat content (HC). The region used to explore each of these variables is between 170°W and 70°W in longitude and from 15°S to 15°N in latitude.

a) Physical variables

(1) Entrainment velocity anomaly

The entrainment velocity is the upward velocity at the base of the mixed layer. The Entrainment velocity during El Niño years decreases, but in some El Niño years, for example 1896-1897, 1899-1900, 1902-1903, 1913-1914, 1818-1819, and 1940-1941, there is still significant upwelling over small areas. During la Niña years we expect that the entrainment velocity will increase because of increased upwelling. These large values for positive entrainment velocity occurs for the stronger La Niña events of 1916-1917, 1917-1918, and 1988-1989, while for weak La Niña events the increase of the entrainment velocity is not as strong. The composite figures (Figures 1e and 1f) show that entrainment velocity with units of 10^{-6} m s^{-1} for El Niño and La Niña events is very patchy. In addition, during El Niño events downwelling occurs over an area between 170°W and 110°W and 2°S to 2°N, but there is some upwelling at the equator between 110°W and 100°W, and between 4°N to 6°N and 170°W to 120°W. During El Niño events there is both downwelling and some significant upwelling. During La Niña years the upwelling occurs more uniformly with very few small areas of downwelling.

(2) Wind stress anomaly

The same procedure was applied to explore changes of wind stress in the data set during El Niño and La Niña events. Wind stress causes surface divergence, and consequently upwelling due to the principle of consevation of mass. During El Niño events wind stress decreases as a consequence of weaker trade winds due to anomalous westerlies winds producing less divergence, and thus a decrease in upwelling. Every El Niño year shows a westerly wind anomaly with higher westerly wind anomaly corresponding to stronger El Niño. Figure 1c presents the composite wind stress anomaly with units of N m^{-2} during El Niño events and Figure 1d shows the composite of wind stress anomaly during La Niña, when the easterlies are stronger due to a higher presure gradient.

(3) Sea surface temperature anomaly

The SST anomaly shows that the higher warm SST anomalies correspond to the years 1877-1878, 1982-1983, and 1997-1998 in which El Niño event was stronger than in other years. In the case of la Niña the colder anomalies of SST correspond to the years 1916-1917, and 1988-1989 in which La Niña events were strongest. The composite SST for the strongest 24 El Niño events is shown in Figure 1a, and the SST anomaly composite for the 29 strongest La Niña events is shown in Figure 1b. Consistant with previous descriptions of El Niño the plot shows warming of 2.7 °C centered at 140°W. The composite SST anomaly is slightly higher than in other studies because for this research we use strong El Niño years that meet the CHI criteria.

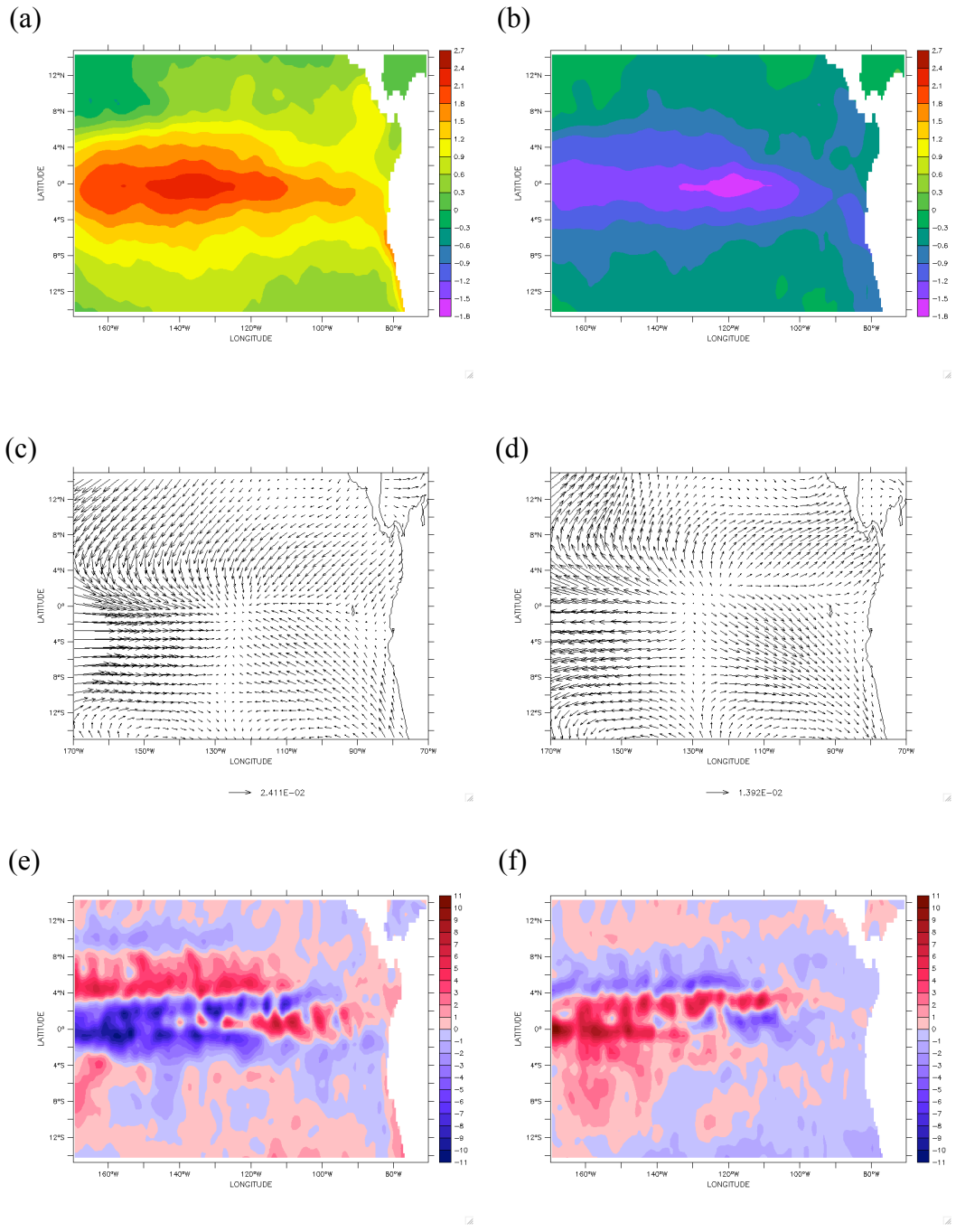

Figure 1. Composite anomalies for El Niño (CHI≥1) of SST (a), TAU (c), and WE (e), and for La Niña (CHI≤-1) of SST (b), TAU (d), and WE (f) in SODA 2.2.4.

(4) Vertical velocity

These results motivate us to construct zonal and meridional sections of vertical velocity (W), to verify and understand the structure and behaviour of vertical velocity at the base of the mixed layer. The plots for vertical velocity have a factor of exageration of 10^6 m s^{-1}. The zonal vertical section of vertical velocity anomaly (Figure 2a) plotted for the composite La Niña at 0° latitute shows dominant upwelling in the western and central Pacific Ocean from 170°W to 110°W, whereas in the eastern Pacific downwelling is dominant and there are very small areas of well-defined upwelling. At 2°N the zonal section shows dominant upwelling mainly in the upper 200m, at this latitute the upwelling extends from 170°W to 80°W (see Figure 2b).

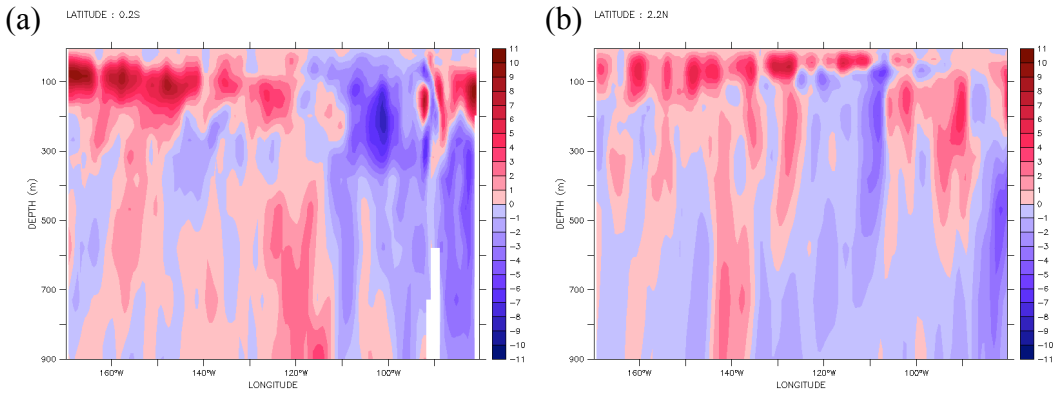

Figure 2. Zonal sections for La Niña (CHI≤-1) at 0° lat. (a), and 2° N lat. (b) of the composite W anomaly in SODA 2.2.4.

At depths from 200 m to 900 m upwelling is dominant in the western and eastern Pacific, while in the Central Pacific downwelling is dominant. The meridional sections between 15°N and 15°S mainly show dominant upwelling at 140°W, while at 110°W,

150°W, and 160°W there are some areas of downwelling that extend from the surface to 900m, and other areas show upwelling from 300m to the surface at 150°W and 160°W (Figure 3).

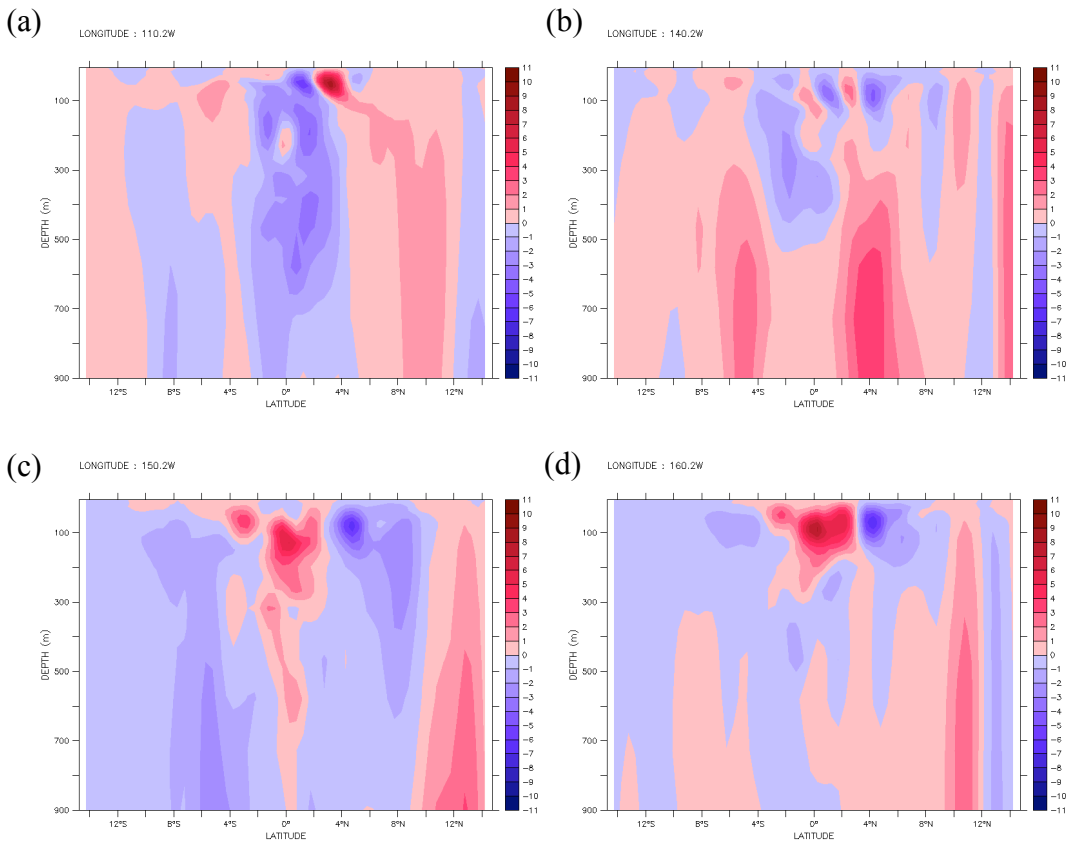

Figure 3. Meridional sections for La Niña (CHI≤-1) at 110°W (a), 140°W (b), 150°W (c), and 160°W (d) longitude, of the composite W anomaly in SODA 2.2.4.

Vertical sections of the vertical velocity anomaly for the El Niño composite were plotted in Figure 4. Zonal sections at latitudes of 2°S,0°,2°N, and 4°N have a

dominant downwelling over the equatorial Pacific Ocean, although there are some significant areas of upwelling located in the eastern Pacific.

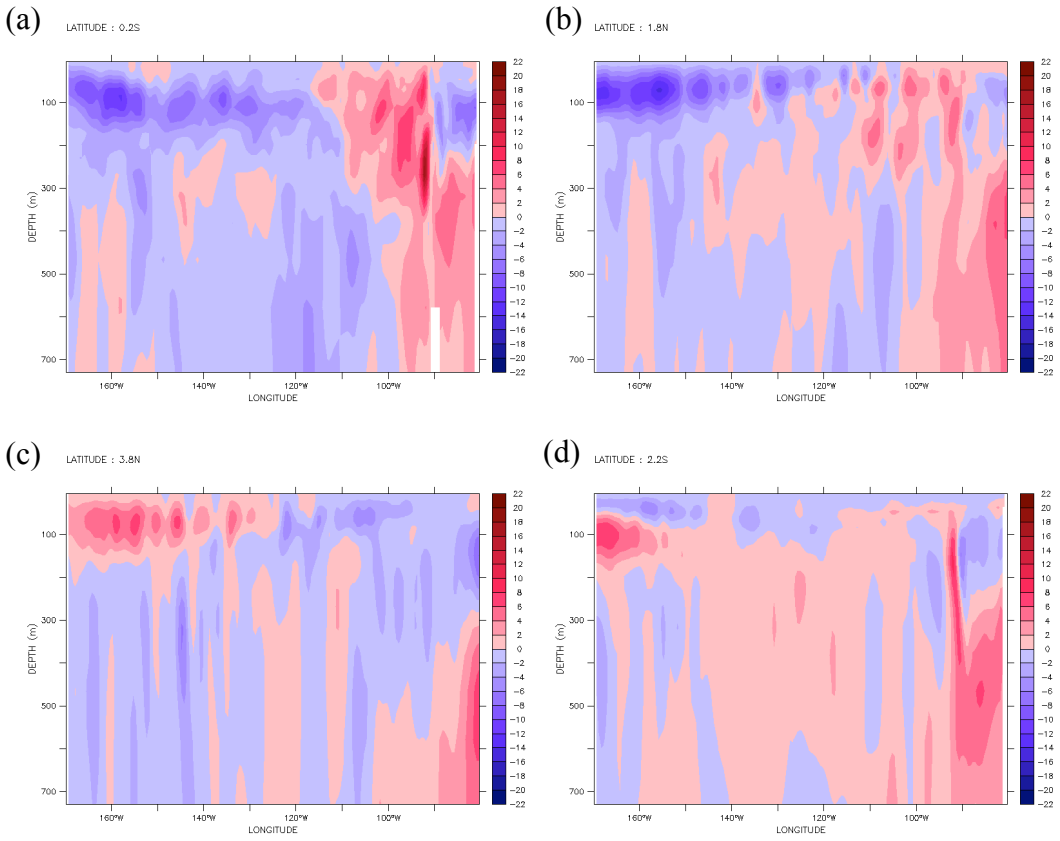

Figure 4. Zonal sections for El Niño (CHI≥1), at 0° (a), 2°N (b), 4°N (c), and 2°S (d) latitude, of the composite W anomaly in SODA 2.2.4.

At latitudes 2°S, 0°, and 2°N, the areas of upwelling extend from 100°W to the coast of South America. The vertical section at 4°N is quite different, showing significant upwelling in the western Pacific from 170°W to 140°W, and some positive deep vertical velocity anomalies around 80°W in the eastern Pacific. Meridional sections between 15°S and 15°N have been plotted for 110°W,140°W,150°W, and

160°W. These meridional sections, presented in Figure 5, show dominant downwelling over the Pacific Ocean, with several very small patchy areas of upwelling. The strongest upwelling is located at 150°W longitude between 4°N-8°N.

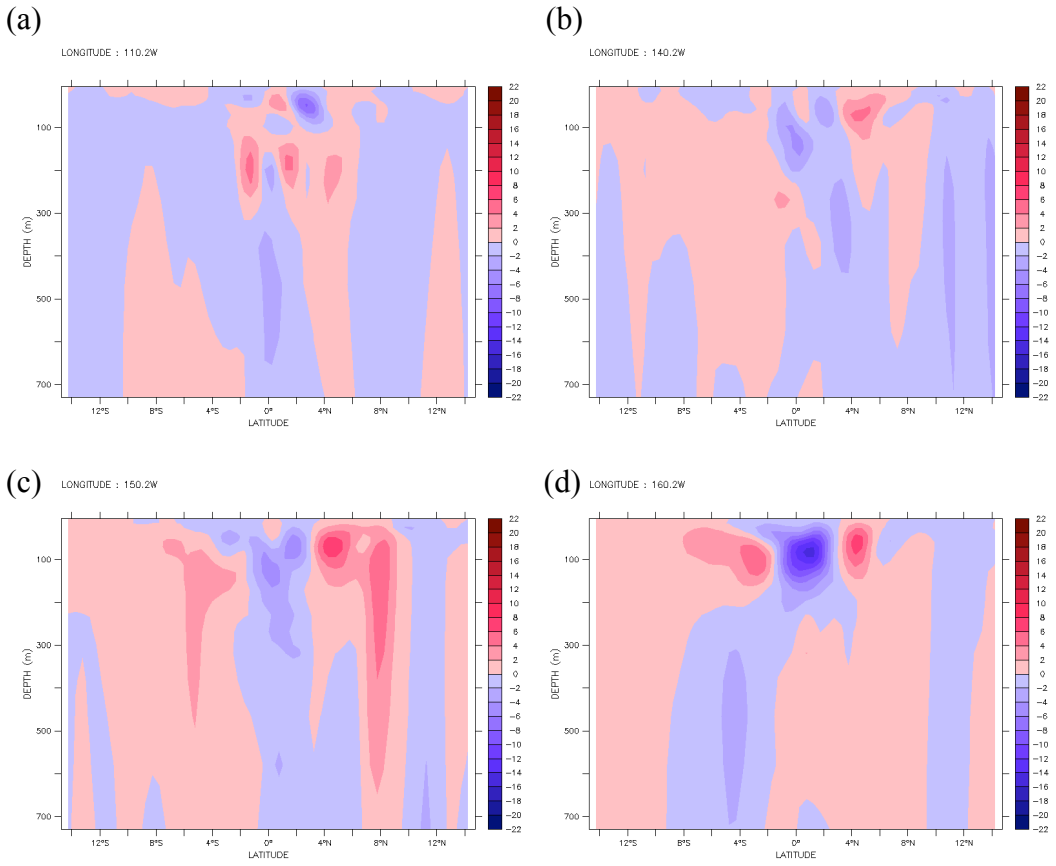

Figure 5. Meridional sections for El Niño (CHI≥1), at 110°W (a), 140°W (b), 150°W (c), and 160°W (d) longitude, of the composite W anomaly in SODA 2.2.4.

(5) Mixed layer depth

The criteria used to find the mixed layer depth is based on differences in density. The mixed layer depth is determined as the depth at which the difference in density relative to the surface is equal to 0.3 kg m^{-3}. Figures 6a and 6b show the composite

mixed layer depth for El Niño and La Niña within the region between 15°S and 15°N. During El Niño events the eastern equatorial Pacific Ocean off the coast of Ecuador becomes warmer and the thermocline deepens. This is apparent in Figure 6a which shows that the mixed layer depth in the eastern Pacific Ocean has the lowest values at approximately 12m depth and in the western Pacific the mixed layer depth is approximately 104m. In the case of the composite La Niña events the thermocline shoals in the eastern Pacific, and deepens in the western Pacific. The mixed layer depth for La Niña case is located at 5m depth in the eastern Pacific, and in the western Pacific at 145m (see Figure 6b).

(6) Wind stress curl

The wind stress curl anomaly composite covering the area between 15°S-15°N and 170°W-70°W shows that during El Niño there are higher positive values in the area between 0° to 8°N extending from 170°W to around 140°W. From the positive wind stress curl anomaly we can infer that downwelling is occurring over this area. The negative values are associated with areas of upwelling produced by wind stress curl. In Figure 6c, we can see the some upwelling occurs at about 0° to 15°S in the western equatorial Pacific, and in a thin strip along the coast of South America covering the coast of Chile and Peru, which is associated with coastal upwelling over this region. During La Niña, the composite wind stress curl anomaly (Figure 6d) has a negative wind curl anomaly over the area between 4°N and 8°N and between 170°W and 130°W. In this area there is upwelling during La Niña events.

However, is important to note that these areas of wind curl anomaly are located away from the eastern equatorial Pacific.

b) Thermodynamic variable

(1) Heat content

We also explored changes in heat content. Figures 6e and 6f show the heat content composite for El Niño and for La Niña. Heat content is calculated by integrating temperature anomalies from the surface to 100m depth. The heat content in the equatorial Pacific for composite El Niño events shows positive values that vary between 200°C m and 260°C m. The main heat content anomaly extends from 5°S to 5°N and over the whole Equatorial Pacific.

For the case of the La Niña composite, the values of heat content are between -100°C m and -180°C m, and again the most significant heat content anomaly extends over the whole equatorial Pacific between 4°S and 4°N.

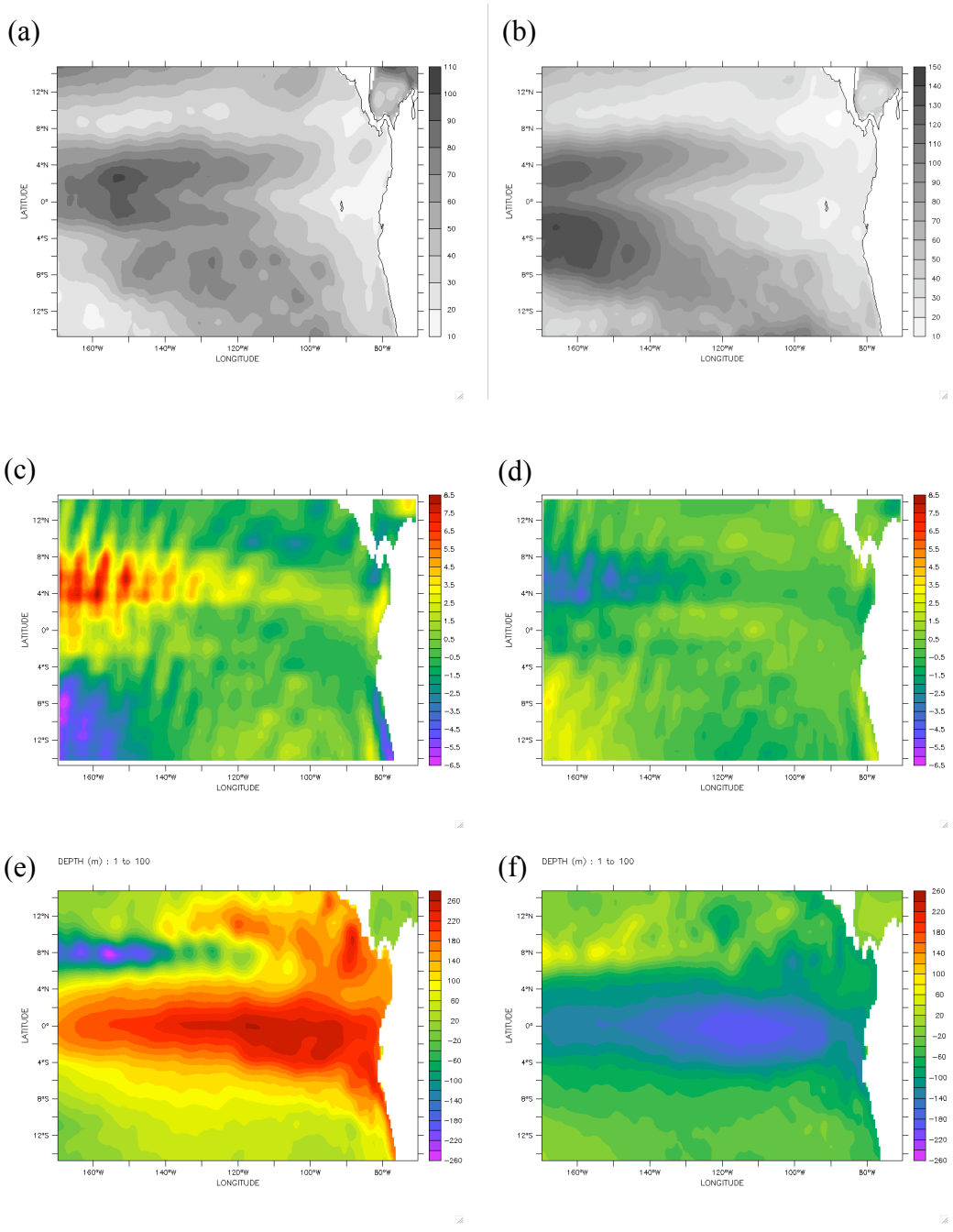

Figure 6. Composite figures for El Niño (CHI≥1) of mixed layer depth (a), wind stress curl anomaly (c), and heat content anomaly (e), and for La Niña (CHI≤-1) mixed layer depth (b), wind stress curl anomaly (d), and heat content anomaly (f) in SODA 2.2.4.

C. Correlation of the center of heat index and entrainment velocity

Based on the methodology proposed by *Giese and Ray* [2011] in their attempt to find a more representative index to measure El Niño, we calculate the amplitude, longitude and area of upwelling. To do this, we calculate upwelling using vertical velocity anomalies at the base of the mixed layer, which are defined as entrainment velocity anomalies. A factor of exageration of 10^5 is applied to compute the amplitude of entrainment velocity, and the units of the amplitude are m s^{-1}. Three methods are used to compute the changes in upwelling during ENSO events. The first method computes upwelling within CHI areas, the second method computes the Center of Upwelling Index (CUI), and the third method computes upwelling in the Niño 1+2 during ENSO events. The methodology applied in the three methods is similar, however the areas and conditions used in each case to calculate the parameters are different and are explained in the following sections.

1. Calculation of upwelling using CHI areas

In this method we use the CHI area to calculate upwelling. The CHI area is calculated based on SST anomalies greater than 0.5°C for the case of El Niño, and less than -0.5°C for La Niña events. The CHI area must be greater than or equal to the area of the Niño 3.4, and has to be located in the tropical Pacific between 120°E to 70°W and 5°S and 5°N [*Giese and Ray*, 2011]. The basis for calculating upwelling over the CHI area is the assumption that anomalously warm SST is mainly due to a decrease in the rate of upwelling during El Niño, while during La Niña the CHI area of anomalously cold SST is because of an increase of upwelling as a result of Ekman divergence.

a) Methodology and criteria used to find the amplitude, longitude and area of the entrainment velocity

The region established to develop this analysis is located from 120°E to 70°W and 5°S to 5°N. For this case areas where changes in upwelling are calculated correspond to the CHI areas, thus the first condition to meet is related to the SST anomalies, and this allows us to associate the calculations of upwelling to ENSO events. Once the areas are determined for El Niño or La Niña events, upwelling is calculated using entrainment velocity anomalies. During El Niño years we determined the amplitude of the entrainment velocity over the CHI area by averaging the negative anomalies of entrainment velocity. The amplitude of entrainment velocity computed gives us a measure of upwelling over the CHI area in which a more negative value reflects a greater decrease in the rate of upwelling.

For La Niña events the same calculation is applied, with the only exception that the CHI areas correspond to La Niña events, and that the amplitude of the upwelling is determined by averaging the positive anomalies of entrainment velocity. The average of positive anomalies of entrainment velocity reflects an increase in entrainment velocity and consequently in upwelling, which is expected to occur during La Niña events when wind stress is strong and the process of Ekman divergence causes an increase in the rate of upwelling, bringing cold water from the deep areas and thus cooling SST.

To compute the longitude of the upwelling we used the same methodology proposed by *Giese and Ray* [2011] to compute CHI, so that the longitude represents the

entrainment velocity–weighted center and is calculated by dividing the sum of entrainment velocity anomalies times the longitude.

b) Three variables that compare the distribution of SST anomaly (CHI)

Figures 7 and 8 show the CHI components calculated using the first methodology for El Niño and La Niña events respectively. The upper panel presents the amplitude of the upwelling multiplied by a factor of 10^5. The middle panel shows the longitude of the entrainment velocity anomalies, and the lower panel shows the area over which upwelling exists.

The entrainment velocity amplitude is plotted in red for El Niño events (Figure 7a) and shows prominent decadal variability during the entire record (1871-2008). The higher peaks in amplitude occur in the early part of the record from 1871 to 1905, and in the last part of the record from 1980 to 1998. The middle part of the record has low variability. This is in general agreement with the results of *Giese and Ray* [2011], who show similar behaviour for SST.

Figure 7b shows the location of negative entrainment velocity anomaly represented by longitude, also showing significant variability. The size of the circles in the plot are proportional to the strength of entrainment velocity anomalies. The strongest negative entrainment velocity anomalies, and thus a greater decrease in upwelling, are located between 160°W and 140°W.

The lower panel in Figure 7c shows the CHI areas, and again the size of the circles again represents the strength of upwelling. There is a tendency that in the early part of the record when the CHI areas are larger the strength of upwelling is greater.

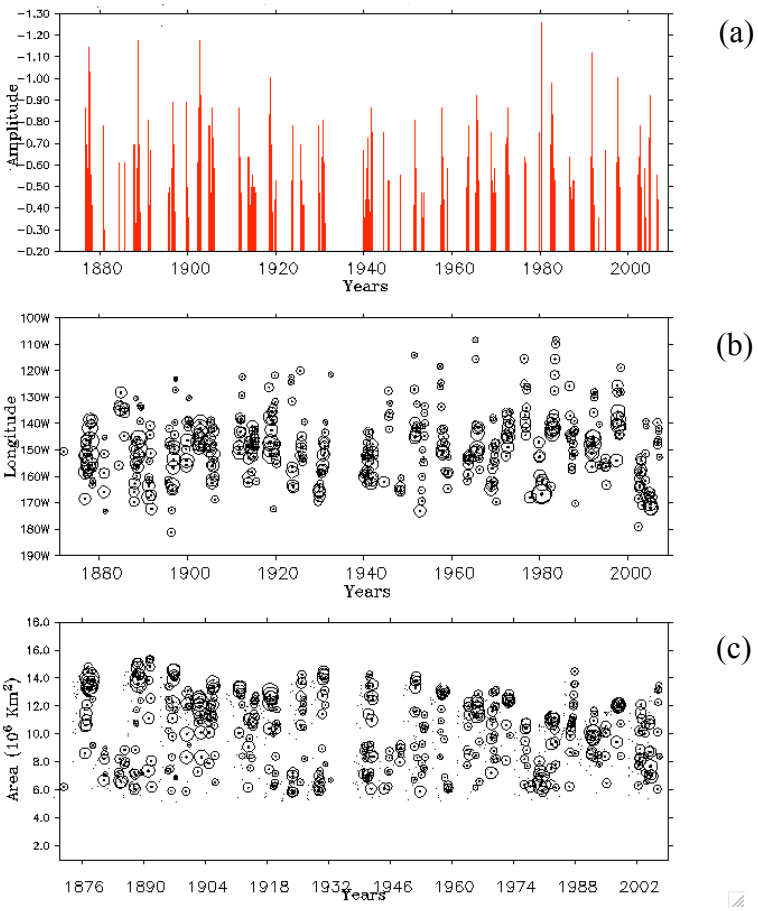

Figure 7. Entrainment velocity anomaly amplitude (a), longitude (b), and area (c) during El Niño events in SODA 2.2.4.

Figure 8 shows the amplitude of positive entrainment velocity anomalies that are related to an increase in upwelling during La Niña. There is also decadal variability in the record, although it is not as strong as during El Niño. The distribution of the location of these anomalies (Figure 8b) is between 180°W to 110°W, with a mean around 155°W. CHI areas are presented in panel 8c and also show the amplitude of upwelling proportional to the size of the circles.

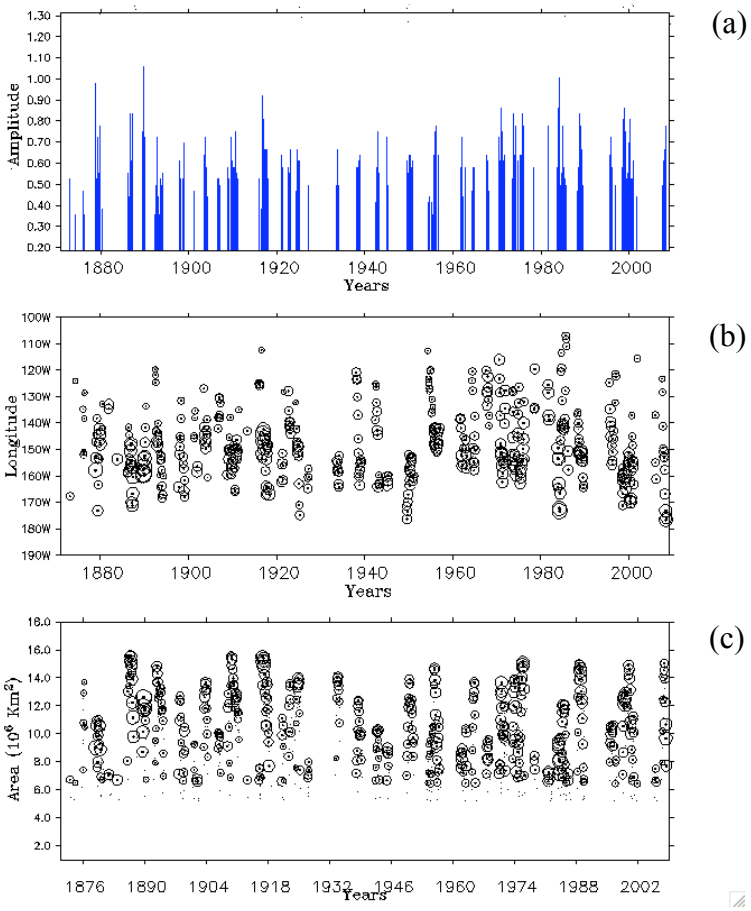

Figure 8. Entrainment velocity anomaly amplitude (a), longitude (b), and area (c) during La Niña events in SODA 2.2.4.

c) Center of heat index and entrainment velocity

We begin by exploring the correlation between CHI amplitude and the amplitude of negative entrainment velocity. Figure 9a shows in red cross symbols a scatter diagram for El Niño events, and the solid line represents the least squares regression. The calculation gives a correlation of 0.13, which means that the amplitudes are not strongly correlated. The trend of the regression allows us to visualize that for smaller SST anomalies the entrainment velocity anomalies are not as large as in the case when

SST anomalies are larger. Although it is clear that upwelling does not explain all of the variance in SST, it is suggestive that upwelling plays a role in the ENSO phenomena.

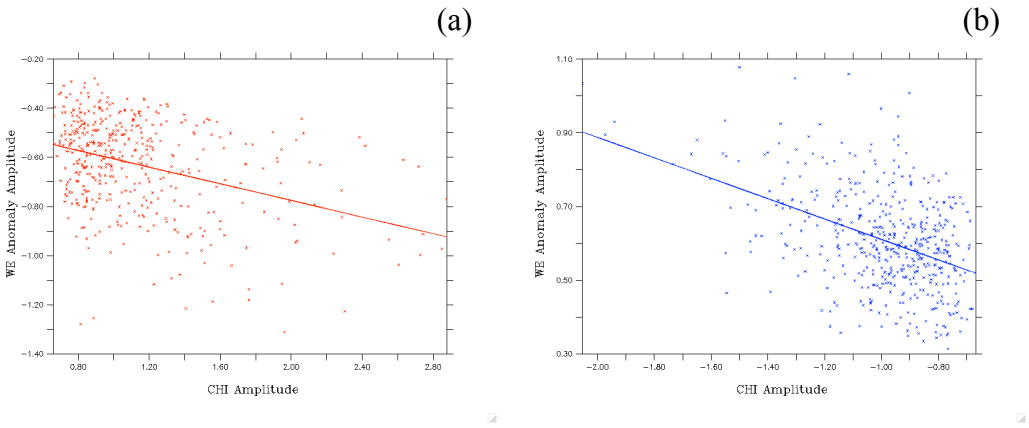

Figure 9. Scatter diagram of CHI amplitude vs. entrainment velocity anomaly amplitude represented for El Niño (a), and for La Niña (b) events.

During La Niña events the correlation between the CHI amplitude and the amplitude of upwelling (positive entrainment velocity anomalies) is a little higher than for El Niño. The least squares regression give a correlation of 0.19, and is shown by a blue line in Figure 9b. The trend shows that during weak La Niña events the amplitude of upwelling is less than in cases when cold SST anomalies are larger and consequently there are strong La Niña events.

Figure 10a contains the time series of CHI amplitude and entrainment velocity anomalies amplitude for El Niño events. Plotting this figure we obtain a better visualization of how the process of upwelling (for El Niño a decrease in upwelling) influences changes in SST during El Niño. There is a clear signature of decadal variability in both time series. However it is also clear that the amplitude of SST

anomalies during El Niño events does not have a direct relationship with the changes in the rate of upwelling.

During the El Niño of 1878 in the early part of the record, the amplitude of warm SST anomalies agrees very well with the amplitude of a decrease in upwelling. We expect very strong El Niño events as measured by SST (i.e. 1888, 1903 and 1920) to have a strong decrease in the rate of upwelling. However the El Niño events that occurred in those years are not as strong as suggested by upwelling anomalies. A similar situation occurs in the last part of the record when the amplitude of SST anomalies during the El Niño of 1997, shows that the amplitude of the negative entrainment velocity anomalies is not large. It is clear that for the El Niño of 1997/1998 some other process is responsible of the strong warming.

Figure 10b presents the time series of CHI amplitude and upwelling for La Niña events. In contrast with El Niño events there is no obvious relationship between peaks of the amplitude of upwelling and peaks of SST anomalies. Four major peaks of upwelling amplitude are identified in the figure. They correspond to La Niña events that occurred in the years 1879, 1890, 1917, and 1985. These years correspond to strong La Niña events, including the La Niña of 1917 that is the strongest La Niña event of the record.

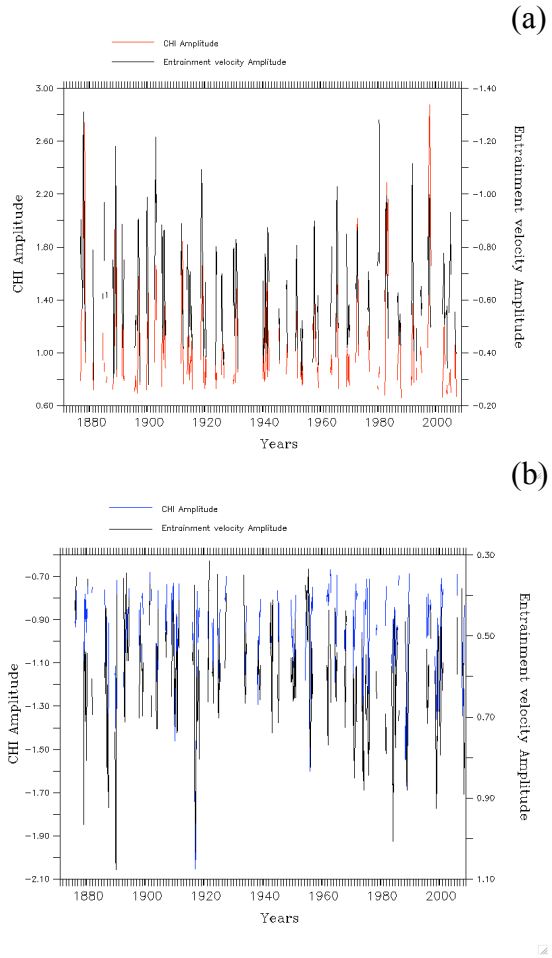

Figure 10. Time series of the amplitude of entrainment velocity anomalies (black), and CHI amplitude represented for El Niño (a), and for La Niña (b) events.

Comparing CHI longitude (temperature weighted center) and the longitude of entrainment velocity anomalies during El Niño and La Niña events, we conclude that for El Niño events (Figure 11a) the location of the temperature - weighted center is eastward of the upwelling - weighted center, which seems to be more westward. It allows us to infer that the higher SST anomalies are not occurring at longitudes where the change in upwelling is strongest. Warm SST anomalies are displaced eastward of the centers of

reduced upwelling. Figure 11b shows a similar situation for the case for La Niña, where the cold SST anomalies are also displaced eastward of the centers of anomalous upwelling.

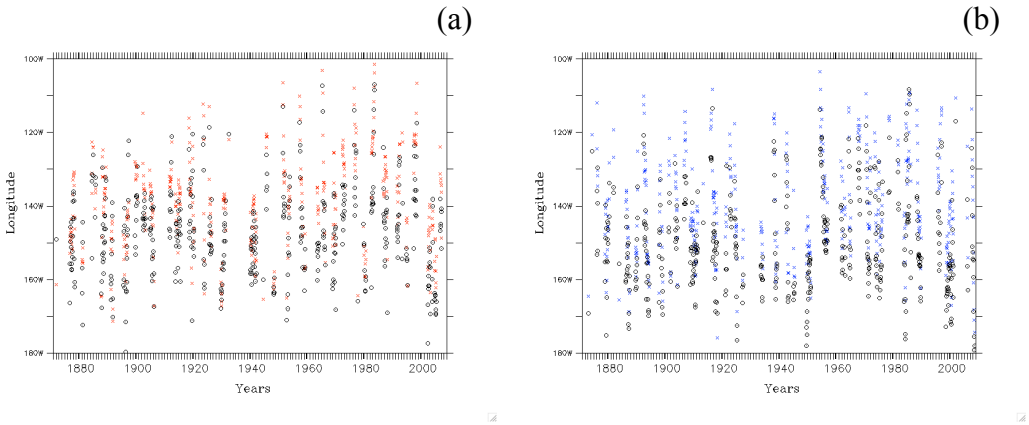

Figure 11. Comparison of CHI longitude (black circles), and entrainment velocity anomaly longitude for El Niño (a) and for La Niña (b) events.

2. Center of upwelling index (CUI)

Since SST anomalies do not occur in the same place as upwelling anomalies we next use a new index to measure the changes in upwelling. The Center of Upwelling Index is calculated using the same procedure as for the Center of Heat Index [*Giese and Ray,* 2011]. ENSO theory explains that changes in SST are mainly due to changes in upwelling during either El Niño or La Niña events. Taking this concept into account we propose a new index. The purpose of this index is to determine if the peaks in upwelling occur at the same time as the peaks in SST, and if these peaks occur over approximately the same area. Three components comprise the Center of Upwelling Index, the CUI amplitude, the CUI longitude and the CUI area.

a) Methodology and criteria used to calculate the index

The area of analysis is the tropical Pacific Ocean from 120°E to 70°W, covering the latitude between 5°S and 5°N; the same area of analysis used to calculate the CHI index [*Giese and Ray*, 2011]. The CUI area corresponds to the area of entrainment velocity anomalies less than -3.0×10^{-6} m s^{-1} for a warm event, and greater than 3.0×10^{-6} m s^{-1} for a cold event, with the constraint that the area of upwelling has to be greater than or equal to the Niño 3.4 area. Because the new metric is not the same as for CHI, upwelling events may not be the same as ENSO events as defined by CHI. Nevertheless, ENSO events are included in these warm and cold states of SST, and we expect greater changes in upwelling during ENSO events.

The CUI longitude parameter gives us the entrainment velocity – weighted center of warming or cooling. The average of entrainment velocity anomalies over the CUI area determines the amplitude of the entrainment velocity anomaly. For the case of warm events, we compute the average of the negative entrainment velocity anomaly, which gives us the decrease in upwelling, while for cold events the positive entrainment velocity anomaly is averaged in order to find the increase in upwelling.

b) Analysis of the amplitude, longitude and area of the CUI

Figure 12 shows the amplitude, longitude and area of entrainment velocity anomalies during warm states. The CUI amplitude reflects the decrease in upwelling that is the responsible for bringing cold water to the surface. The graph shows high variability with peak values in the early part of the record from 1871 to 1920, and in the last part of the record from 1960 to 2008. In the middle of the record variability is less.

The CUI longitude (Figure 12b) shows that the longitude of upwelling is centered between 180°W and 150°W. The size of the circles is proportional to the amplitude of the upwelling and does not show a big difference in the amplitude of upwelling events.

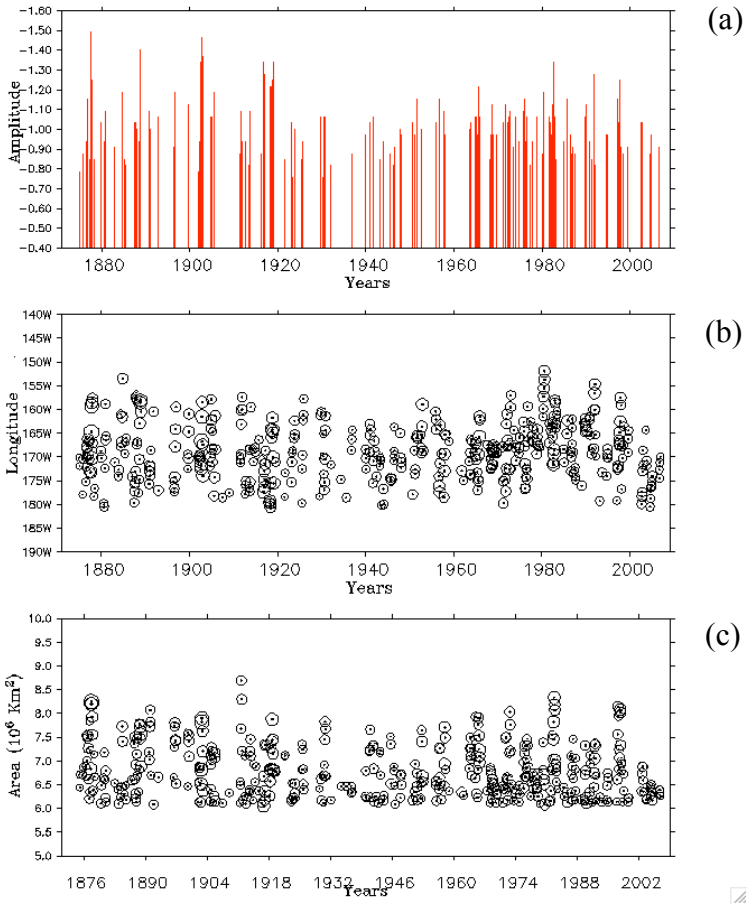

Figure 12. CUI amplitude (a), longitude (b), and area (c) during warm states of SST in SODA 2.2.4.

The distribution of the CHI longitude shows that the location of the entrainment velocity anomalies for the early and last part of the record is more eastward, with a

westward tendency towards the middle of the record reaching a maximum westward location in the 1940's.

Panel 12c shows CUI areas again with the size of the circles representing the strength of CUI. There is no marked trend, and the bigger CUI areas occur during 1876, 1910, 1982, and 1998.

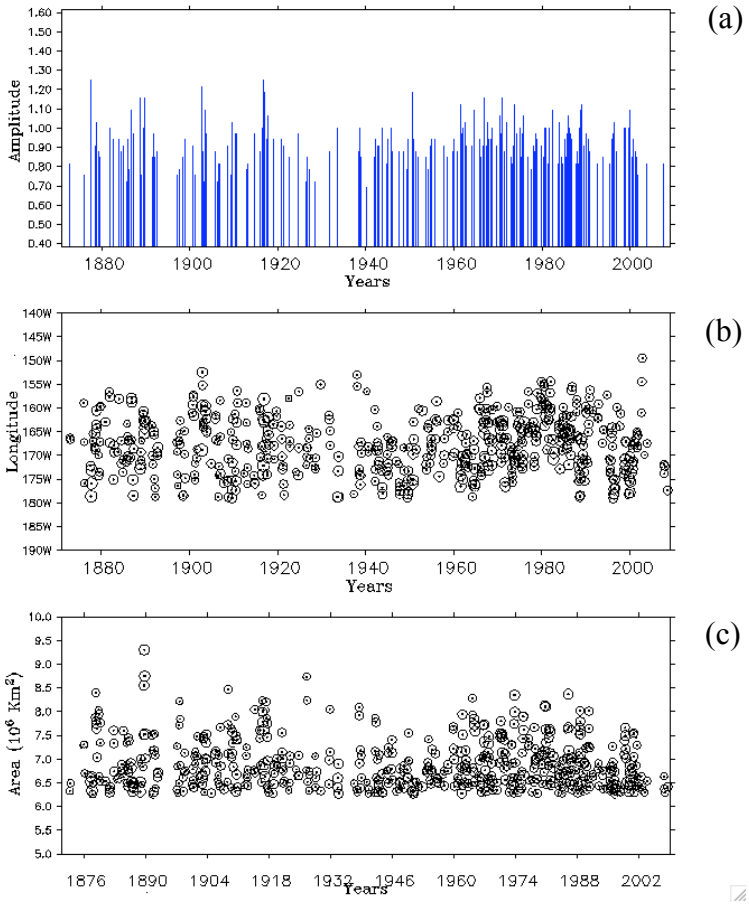

Figure 13. CUI amplitude (a), longitude (b), and area (c) during cold states of SST in SODA 2.2.4.

There is less variability in the amplitude of CUI during cold events (Figures 13a-13c). However, there is a higher occurrence of the CUI index in the last part of the record. The location of the longitudes varies within the same range from 180°W to 150°W as for warm events, and the distribution of the CUI areas is somewhat more dispersed than for warm events. The lower limit in the size of the CUI areas is limited by the condition established to calculate the index, which we specified to be at least the size of the El Niño 3.4 area.

c) Center of heat index and center of upwelling index

In our attempt to find a correlation between CHI and CUI indexes we plot in Figure 14 a scatter diagram of CHI amplitude versus CUI amplitude. For El Niño events (Figure 14a) the scatter of the amplitudes is represented by red crosses, and the red line is the least squares regression. There is a very small correlation of 0.09 between the amplitudes of these indices.

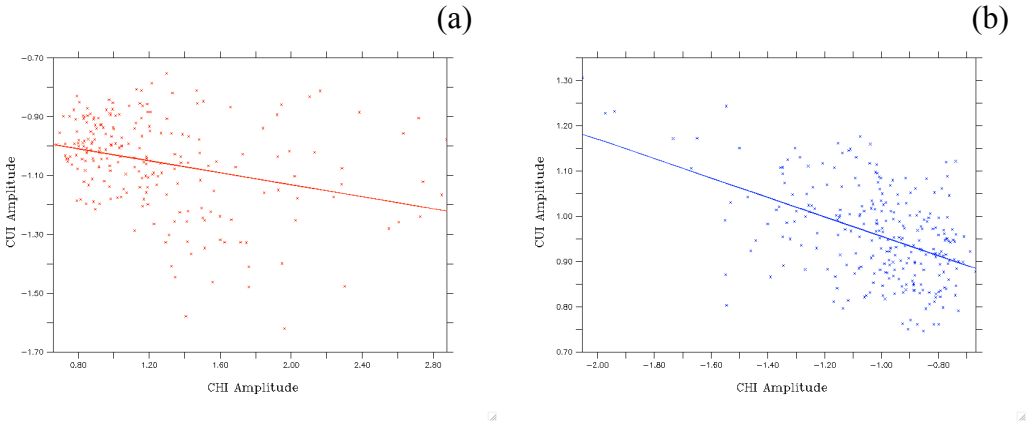

Figure 14. Scatter diagram CHI amplitude vs. CUI amplitude, and correlation represented for El Niño (a), and for La Niña (b) events.

The diagram from the middle of the record to the end is highly variable, so that it is difficult to observe a well-defined trend. The very weak trend shows that during El Niño events when the SST anomalies are higher the amplitude of the negative of entrainment velocity anomalies is more negative, and vice versa.

Figure 14b shows that for La Niña there is a better correlation between the amplitudes of both indices, with a least squares regression of 0.23. In this case we can infer that during La Niña events (cold SST anomalies), the amplitude of upwelling (positive entrainment velocity anomalies) is higher.

A comparison of the amplitude time series of both indices presented in Figure 15a-15b for El Niño and La Niña events shows that the timing of occurrence using either index is similar. Despite the fact that both indices are computed independently the timing of the amplitudes agrees very well.

This suggests that during El Niño, when warm SST anomalies are present, the amplitude of the negative entrainment velocity anomalies (a decrease in the rate of upwelling) is higher. It is clear that the change in the rate of upwelling contributes to SST anomalies for both El Niño and La Niña events. However, strong El Niño or La Niña events do not have a direct relationship to changes in upwelling. Other processes such as zonal advection, or heat fluxes need to be considered.

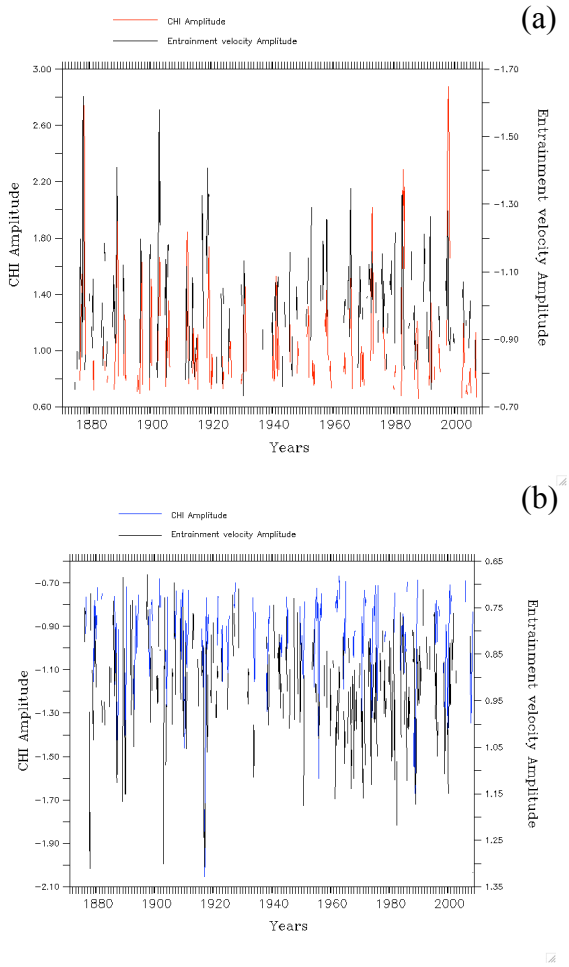

Figure 15. Time series of CUI amplitude (black), and CHI amplitude for El Niño (a), and for La Niña (b) events.

Next we compared the temperature-weighted center and the upwelling–weighted center represented by the longitude of both indexes (Figure 16). The CHI longitudes span a large part of the tropical Pacific, covering longitudes between 180°E to 90°W for both El Niño and La Niña events. However, the distribution of the CUI longitudes is

more compact than for the CHI, ranging over the central Pacific from 180°E to 155°W. The centers of upwelling are generally west of the centers of temperature.

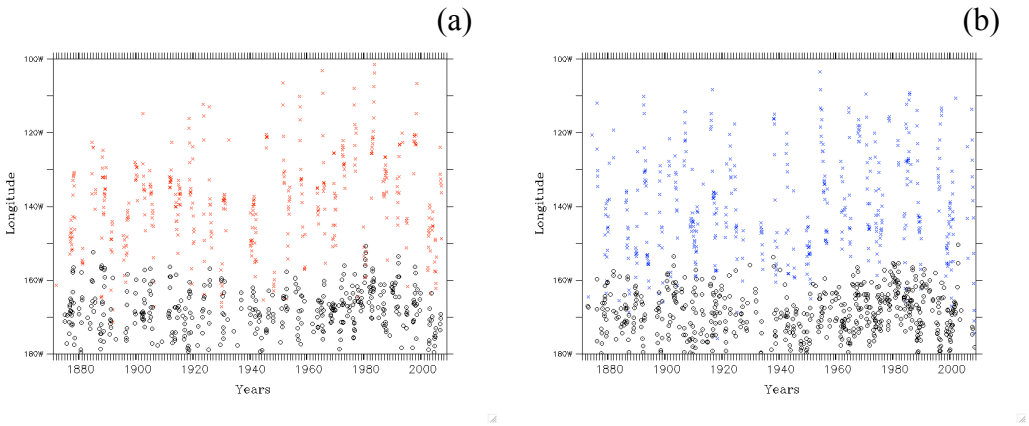

Figure 16. CHI longitude (black circles) and CUI longitude for El Niño (a) and for La Niña (b) events.

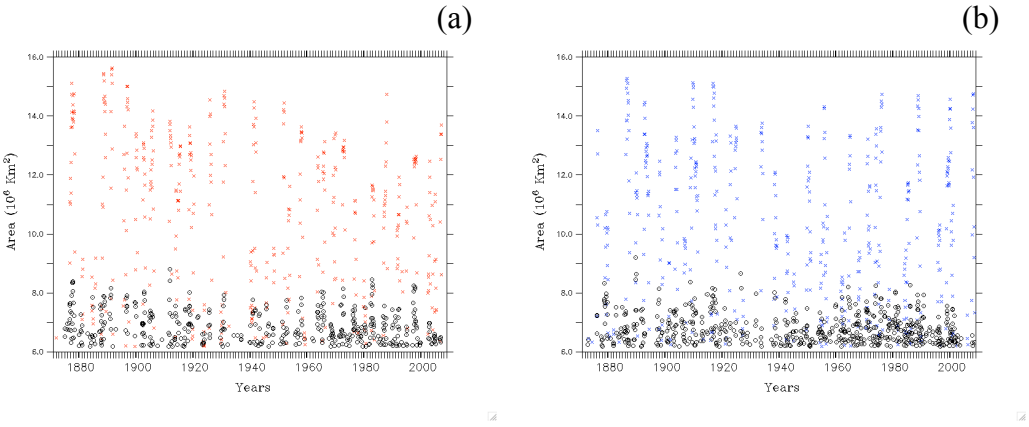

Figure 17. CHI areas (black circles) and CUI areas represented for El Niño (a) and for La Niña (b) events.

Finally, we compare the CHI and CUI areas in Figure 17. The graph clearly shows that CHI areas are much larger than CUI areas for both El Niño and La Niña events. The mean CUI area for both El Niño and La Niña events is approximately 7 x 10^6 km^2, whereas the mean CHI area is around 11 x 10^6 km^2.

3. Calculation of upwelling in the Niño 1+2 Region

We use two different methods to calculate upwelling changes within the Niño 1+2 region during ENSO events. In the first method the occurrence of CHI index is used, such that for every occurrence of a CHI event, upwelling is calculated in the Niño 1+2 region. The second method is a modification of the first one; In this case we consider only the occurrence of El Niño or La Niña events located in the Eastern Pacific Ocean to identify changes in upwelling in the Niño 1+2 region.

a) Methodology and criteria used to calculate upwelling during ENSO events

Upwelling is calculated in the Niño 1+2 region for each month that CHI exists in the tropical Pacific, either for El Niño or La Niña. In this case the area of upwelling is limited to the Niño 1+2 region. In order to determine the amplitude of upwelling in the Niño 1+2 region we select years when ENSO events occur, and then use the entrainment velocity anomalies. For El Niño years upwelling is calculated by averaging the negative entrainment velocity anomalies in order to find the decrease of upwelling, and during La Niña years the amplitude of the entrainment velocity corresponds to the average of the positive entrainment velocity anomalies, which allow us to find the increase in the rate of upwelling.

The entrainment velocity anomaly–weighted center is presented in terms of longitude. Because the area of Niño 1+2 corresponds to the region between 90°W and 80°W, the value of entrainment velocity is calculated within this range of longitudes. This method is not adequate to find a correlation between the ENSO event location in terms of longitude, and the location of upwelling in terms of longitude, because even though some ENSO events occur in the eastern Pacific, others occur in the western or central Pacific, and here we calculate changes in only the Niño 1+2 region.

b) Analysis of the entrainment velocity amplitude and longitude

We analyze only these two parameters because the area used to compute the upwelling was already established as the El Niño 1+2 region. An analysis of upwelling is presented in Figure 18 for El Niño years, and in Figure 19 for La Niña years. Both events are defined using the CHI definition. For El Niño events (Figure 18) the amplitude of negative entrainment velocity anomalies (in red) has low variability for most of the record, although the amplitude of upwelling reaches the largest negative values between 1960 and 1980. The amplitude of upwelling showed in the figure has a factor of exaggeration of 10^5.

The locations of entrainment velocity anomalies are limited to the longitudes covered by the Niño 1+2 region (90°W-80°W), and the size of the circles represents the amplitude of upwelling. During the last part of the record (Figure 18b) the amplitude of negative entrainment velocity anomalies is greatest. These peaks in amplitude of upwelling are located across the full range of longitudes of the area of study.

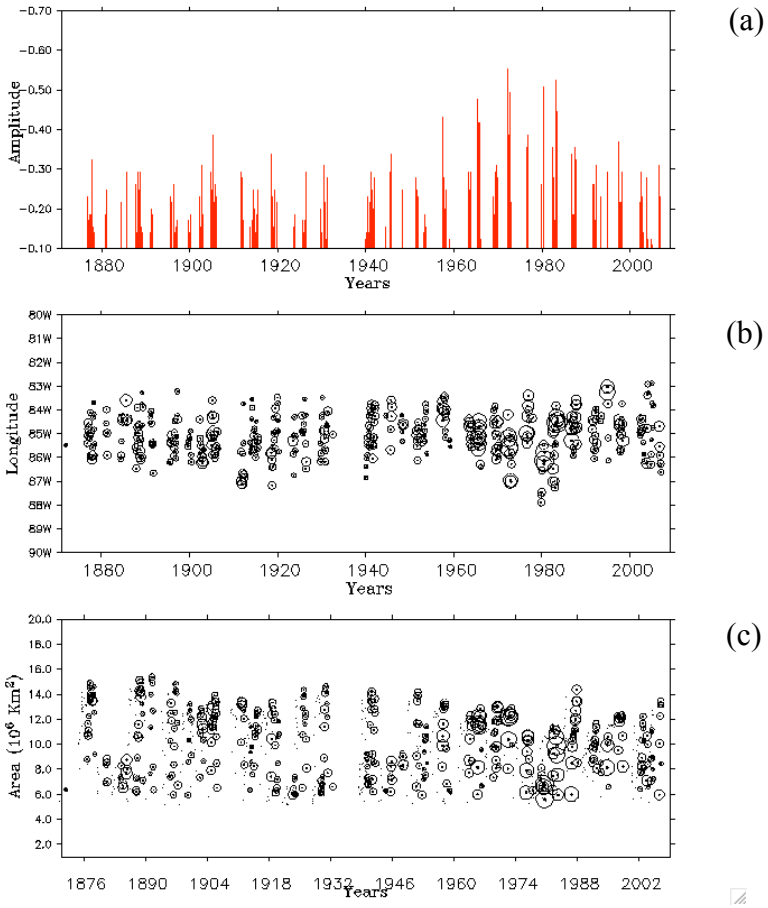

Figure 18. Entrainment velocity anomaly amplitude (a), longitude (b) in the Niño 1+2 region, and CHI area (c) during El Niño events in SODA 2.2.4.

For La Niña, shown in Figure 19, the amplitude has greater variability than in the case of El Niño, although the values of amplitude are lower for this case. Three peaks in amplitude are observed in the record, one before 1920, the second after 1980 and the last before 2000. Panel b of Figure 19 shows the location of upwelling within the same area (the Niño 1+2 region), again with the size of the circles representing the amplitude of the negative entrainment velocity anomalies during La Niña events. There is a slight tendency for strong upwelling events to occur in the period from 1960 until 2000.

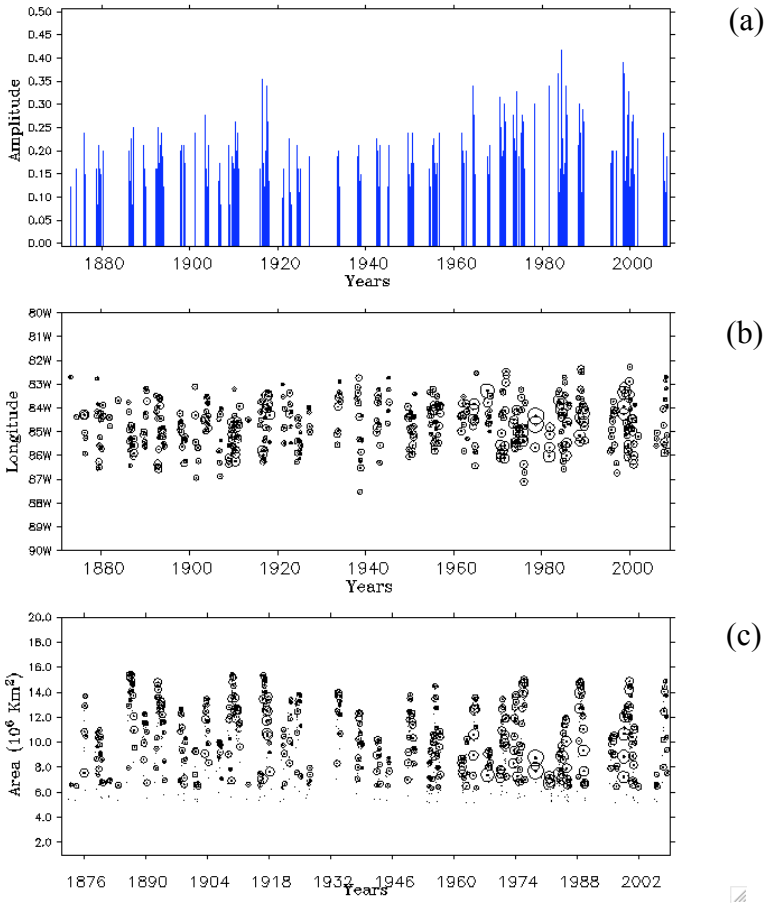

Figure 19. Entrainment velocity anomaly amplitude (a), longitude (b) in the Niño 1+2 region, and CHI area (c) during La Niña events in SODA 2.2.4.

c) Correlation of center of heat index and entrainment velocity in the Niño1+2 region

In order to assess changes in upwelling within the Niño 1+2 region during El Niño events, we plotted the CHI amplitude versus the amplitude of the negative entrainment velocity anomalies over the Niño 1+2 region (See Figure 20a). The red line shows the correlation found using a least squares regression. This regression gives a very weak correlation of just 0.023. One of the constraints of this method comparing

CHI amplitude and the amplitude of decreasing in upwelling in the Niño 1+2 region is that here we compare El Niño events that occur over the whole tropical Pacific Ocean with changes in upwelling over a relatively small region in the eastern Pacific. However this comparison is important in order to verify that there are impacts in the Niño 1+2 region even with El Niño events occurring in the western Pacific.

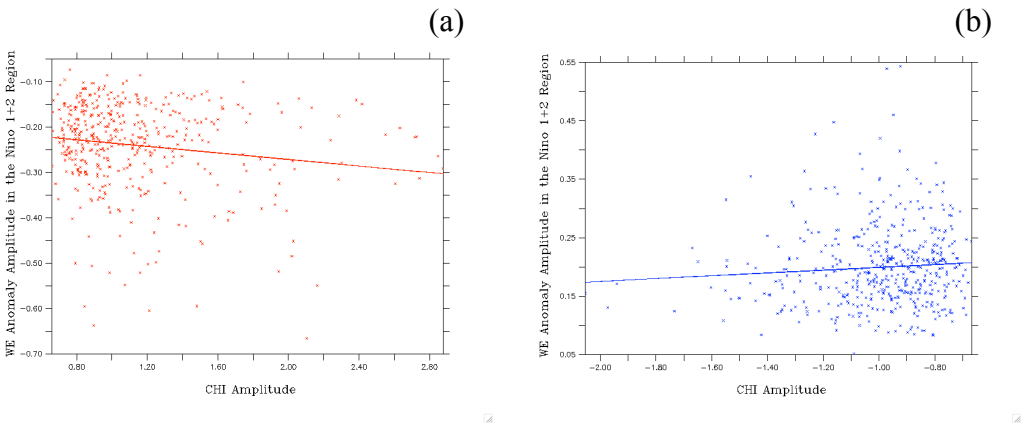

Figure 20. Scatter diagram of CHI amplitude vs. entrainment velocity anomaly amplitude in the Niño 1+2 region for El Niño (a), and La Niña (b) events.

We use the same technique for the case of La Niña events, shown in Figure 20b. The correlation for this case is even weaker, at just 0.0053. The same limitation present for the case of El Niño is also present for La Niña.

Despite the low correlation we plot a diagram comparing the time series of CHI amplitude and the amplitude of upwelling in the Niño 1+2 region for El Niño (Figure 21a) and La Niña events (Figure 21b).

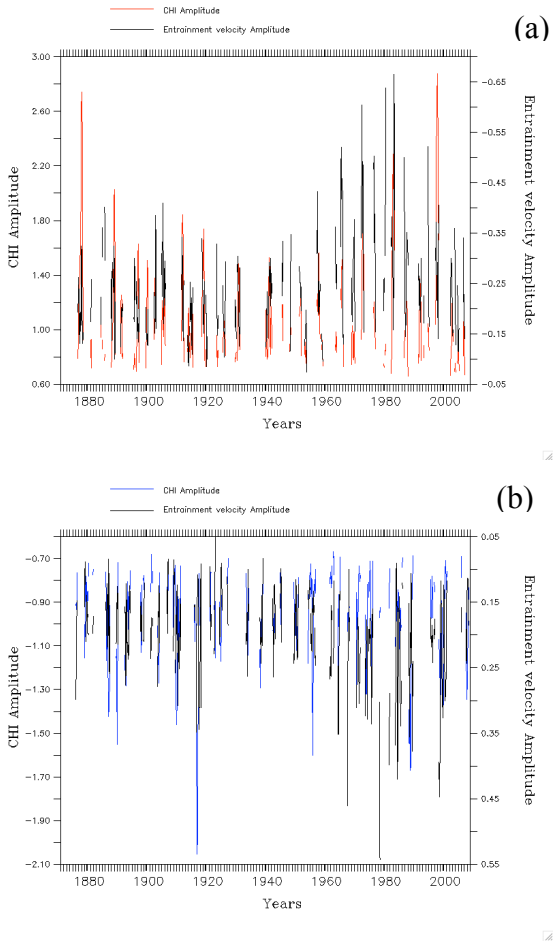

Figure 21. Time series of amplitude of the entrainment velocity anomalies (black) in the Niño 1+2 region, with CHI amplitude for El Niño (a), and for La Niña (b) events.

The results show that only during the part of the record from 1960 to 1980 both time series agree very well, while for the rest of the record there is almost no correlation. This analysis is an indicator that only eastern Pacific El Niño events have a good correlation. In fact during La Niña events the amplitude of upwelling and CHI agree very well during 1876 and 1999-2000 La Niña events.

d) Methodology and criteria used to calculate upwelling during east Pacific ENSO events

The first part of this analysis is carried out using a method similar to the one used to calculate the Center of Heat Index [*Giese and Ray,* 2011]. Here we calculate the index limiting values to ENSO events that are located in the eastern Pacific. Thus the area established for the analysis is from 140°W to 80°W, and between 5°S and 5°N. The El Niño CHI east index (modified CHI) exists if the area of SST anomaly > 0.5° C is greater than the Niño 3.4 region. For La Niña the condition is that the SST anomaly has to be less than -0.5°C. The CHI east index areas are obtained following this procedure, and consequently they have limited size.

The amplitude of CHI east is determined by averaging SST anomalies over the CHI east areas. It is calculated by multiplying the sum of SST anomalies times the CHI east area, and dividing by the sum of the CHI east area. The third CHI east component is the longitudinal center of heat. It represents the temperature–weighted center, and is calculated using the same procedure as for CHI longitude.

e) Analysis of CHI east amplitude, longitude and area

The upper panel of Figure 22 shows the amplitude of the upwelling based on the negative entrainment velocity anomalies. The distribution has moderate variability with an increase of amplitude between the years 1960 and 1990. Figure 22b shows the location of negative entrainment velocity anomalies in terms of longitude.

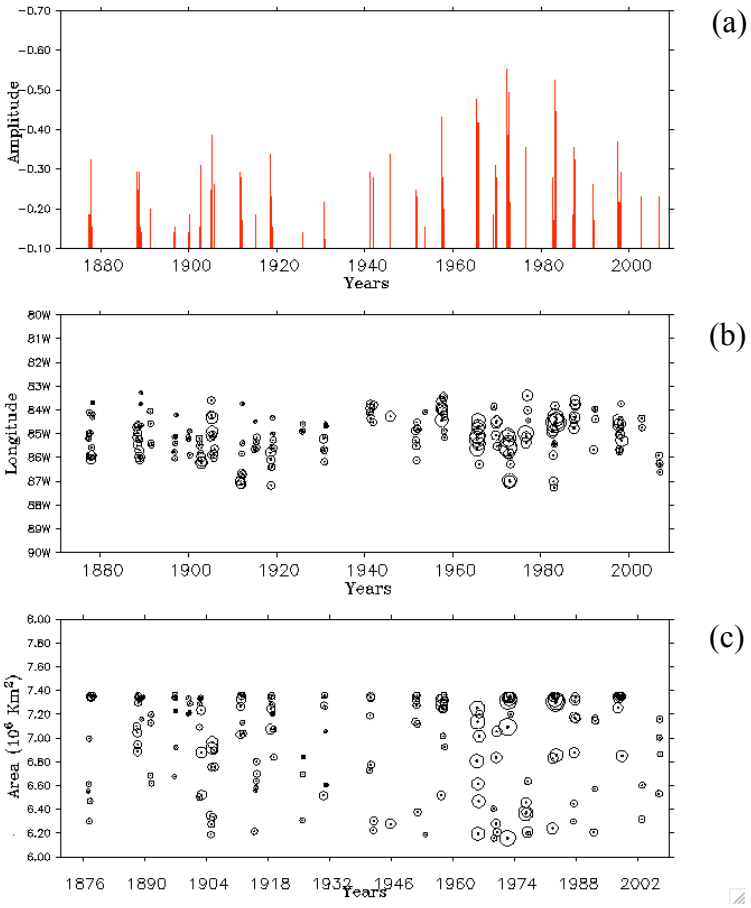

Figure 22. Entrainment velocity anomaly amplitude (a), longitude (b) in the Niño 1+2 region, and CHI east area (c) during El Niño events in SODA 2.2.4.

Warm events are located across the whole range of the area of study, with little discernable change across the record. The CHI east areas are presented in Figure 22c. Again, there is little trend of the size of upwelling events across the record.

CHI east for La Niña was analyzed as well. The amplitude of upwelling was computed by averaging the positive entrainment velocity anomalies. The distribution of CHI east amplitude is presented in Figure 23.

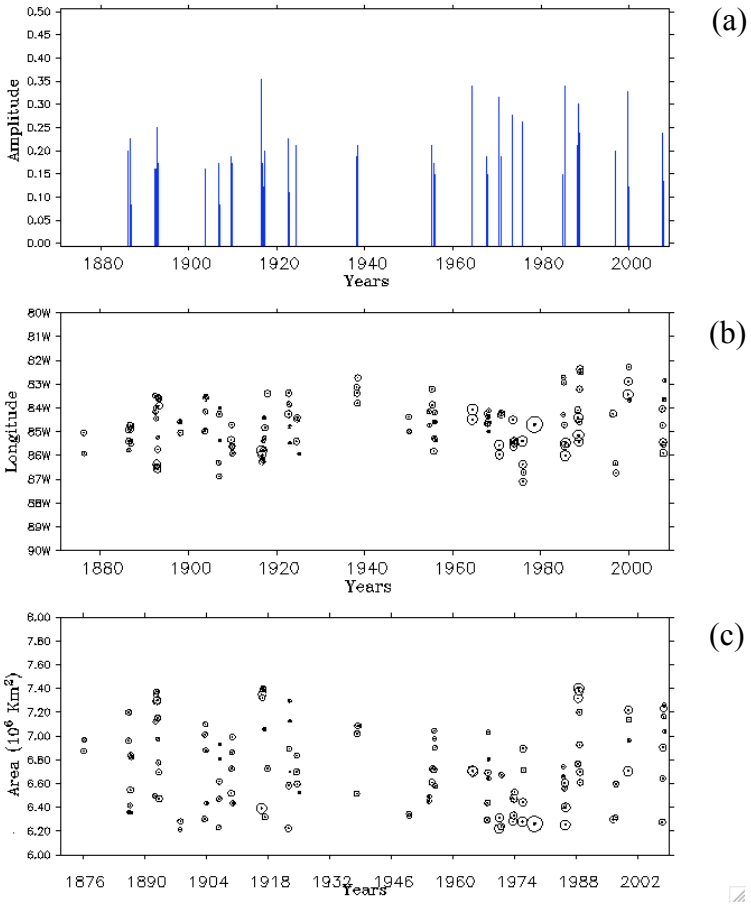

Figure 23. Entrainment velocity anomaly amplitude (a), longitude (b) in the Niño 1+2 region, and CHI east area (c) during La Niña events in SODA 2.2.4.

The La Niña case shows less variability than for El Niño and there is not a marked change in amplitude. The longitude during the period from 1960 to 1990 varies between 90°W and 80°W, showing little trend or even variability. Figure 23c shows the area of upwelling during La Niña CHI. As for the other components there is little trend or variability in the size of the upwelling area.

f) Correlation of CHI east and entrainment velocity in the Niño1+2 region.

The correlation between SST anomalies and changes in upwelling during ENSO events is presented in Figure 24, which contains a scatter diagram of amplitude of CHI east and the amplitude of upwelling in the Niño 1+2 region. We anticipated a high correlation between these measures, since we select only El Niño events that occur in the eastern Pacific. However the results shown in Figure 24a for the case of El Niño events give a correlation of just 0.024. There is no correlation for La Niña events (Figure 24b).

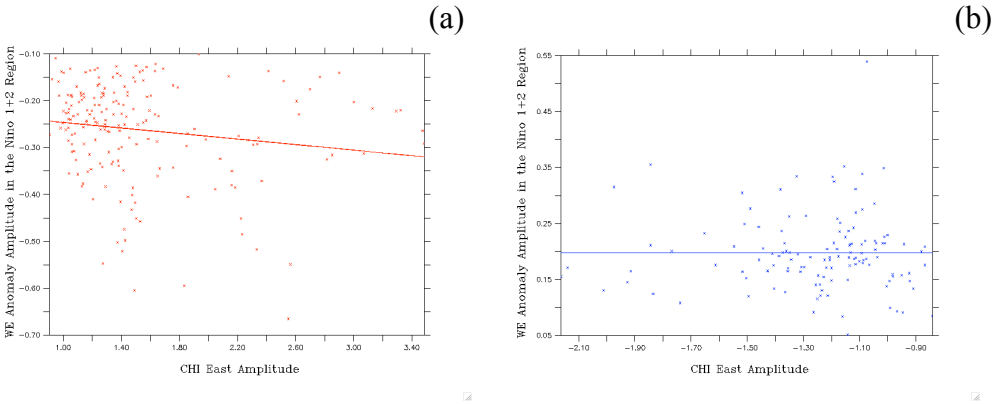

Figure 24. Scatter diagram of Entrainment velocity anomaly in the Niño 1+2 region and CHI east amplitude. The least squares regression is shown as a line for the El Niño (a), and La Niña (b) events.

The amplitude time series for CHI east and upwelling in the Niño 1+2 region is shown in Figure 25. The plot shows that these amplitudes agree only for the years from 1958 to 1982. Before this time there is little association between upwelling strength and the strength of El Niño.

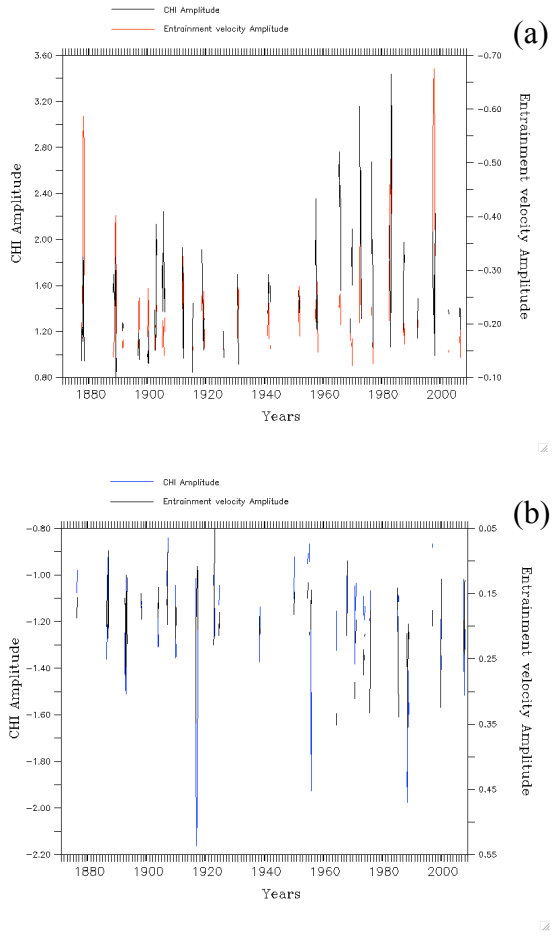

Figure 25. Time series of amplitude of the entrainment velocity anomalies (black) in the Niño 1+2 region, and CHI east amplitude for El Niño (a) and for La Niña (b) events.

From 1958 onward there are El Niño events that are prominently in the Eastern Pacific 1957-1958, 1969-1970, 1972-1973, 1982-1983, and 1997-1998. Interestingly the 1969 El Niño has a strong upwelling anomaly but relatively little SST warming. The La Niña CHI east amplitude and amplitude of upwelling are shown in Figure 25b. There are three specific years (1889-1890, 1917-1918, and 1988-1989) that correspond to three strong La Niña events.

D. Center of heat index and fisheries

1. Fisheries records for the area of study

As part of our study we explore the impact of ENSO events on the fisheries industry for countries that are affected by changes in the Niño 1+2 region. This analysis is based in the fact that changes in upwelling during ENSO events alter the amount of nutrients in the coastal east Pacific. During El Niño events there is a decrease in the rate of upwelling so fewer nutrients are upwelled, and consequently the productivity is reduced which ultimately impacts the fish population. During La Niña events the rate of upwelling increases bringing more nutrients from the deep ocean resulting in an increased fish population.

For this analysis we used fisheries data available online from Ecuador and Peru. The data consist of annual fish catch for each country. These data sets are provided by their respective national web pages. In Ecuador the organization in charge of fisheries management is the *Instituto Nacional de Pesca* (INP), and in Peru the organization in charge of managing fisheries resources is the *Instituto del Mar del Peru* (IMARPE). Both agencies perform similar functions and they are in charge of keeping fisheries data up-to-date. We obtained data from these two countries and compared it with CHI indices data.

The purpose of this analysis is to assess the impacts of ENSO on the size of fish catch because of its importance to the economies of Ecuador and Peru.

2. Limited data

The goal was to obtain at least a time series of fisheries data comparable with CHI, a record that spans 138 years. However in both cases this was not possible since the records cover shorter periods of time. In the case of Ecuador the time series are subcategorized into large pelagic fish, small pelagic fish, and sharks. The subcategory large pelagic fish covers a short period from just 2004 to 2010, the small pelagic fish subcategory covers from 1981 to 2009, and the shark category covers from 2004 to 2010. In order to be able to identify changes in fisheries in Ecuador we use only the subcategory small pelagic fisheries that covers a longer period compared with the other two categories. The Peru fisheries data used for the analysis covers the period from 1950 to 2009, and includes pelagic fisheries species in general.

An issue of concern is that the fisheries data for both cases (Ecuador and Peru) is yearly data, while CHI data is monthly data, so the changes in upwelling due to ENSO events may not be reflected for those years in which within a calendar year an El Niño and La Niña event occurs.

3. Main species present in the area

In Ecuador the following species are monitored: anchovy, crevalle jack, round sardine, chub mackerel, and alewife. The Peru database includes the following pelagic species: anchovy, tuna, jurel, sardine, bonito, chub mackerel, peruvian rock seabass, skipjack, gurnard, hake, mullet, pacific sanddab, smalltooth sawfish, and other minor groups. The fisheries species have different biological behavior and thus react differently to ENSO. However, we evaluate the changes observed in the total number of

catches of fish for the whole species because of the difficulty of identifying the individual impact. The main changes in the fish population are due to change in temperature and the availability of nutrients related to changes in upwelling. Both conditions might affect the patterns of migration of some species, as well as possibly interfering with development of the species in terms of size and fitness that may affect the populations of fish available for the industry.

4. CHI and changes in populations of fish off Ecuador and Peru

The CHI and fisheries data is presented in Figure 26. Peru fisheries data is multiplied by a factor of 4 x 10^{-6}, and the Ecuador fisheries data by a factor of 10^{-6}. Both fisheries data sets have units of Tons.

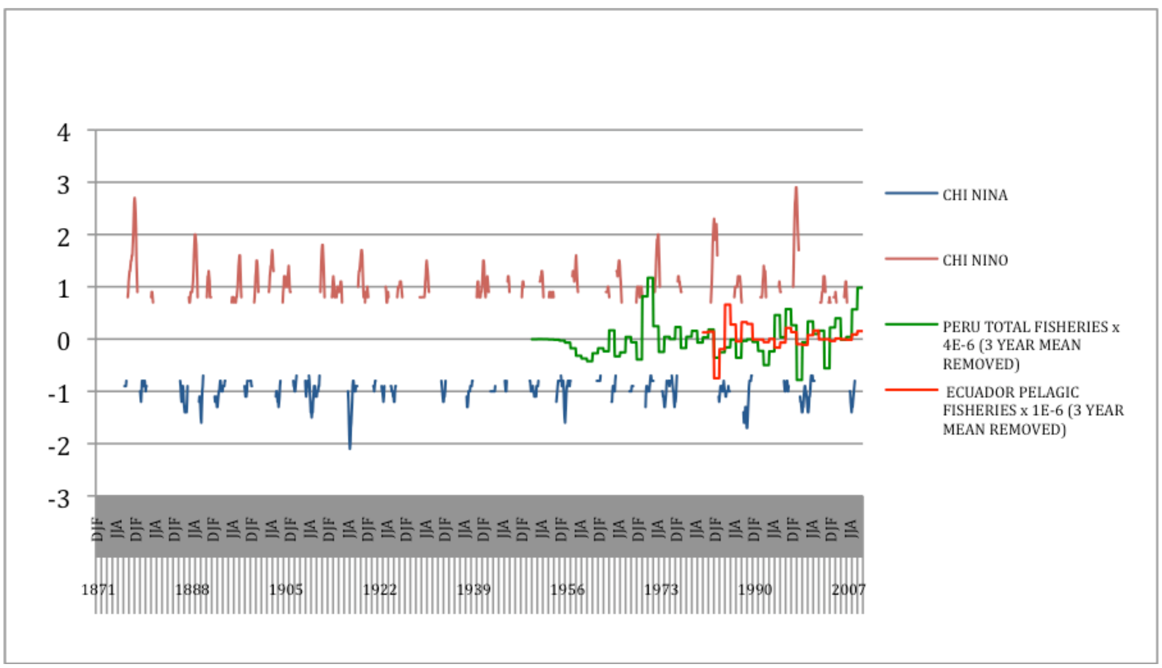

Figure 26. CHI and Ecuador and Peru Fisheries.

The annual fisheries data obscures the changes during ENSO events, especially in those years when there are El Niño and La Niña events in the same calendar year. Nevertheless, based on the data available, there is an identifiable change in the populations of fish in both countries due to ENSO. For both fisheries data sets we removed the three-year mean in order to remove the high frequency variability. The data is re-plotted in Figure 27 for the period from 1950-2008 to emphasize the period for which there is more fisheries data.

During the first part of the record, from 1950 to 1981, the analysis has only Peru fisheries data and CHI amplitude, since the Ecuador fisheries data begins in 1981. In this part of the record the Peru fisheries catches and CHI amplitude agree well, showing that during El Niño events, when SST is warm and upwelling decreases, the impact is to cause the populations to decrease, whereas for La Niña, when there is cold SST and the rate of upwelling increases bringing up more nutrients, the populations of fish increase.

The Peru fisheries data is too sparse to indentify a response to the El Niño events of 1951-1952 and 1953. During the next El Niño event, in 1957-1958, the impact of El Niño is more clear, showing a decrease in population of fish. Interestingly this decrease in population extends until 1960. The El Niño of 1963-1964, which is not a very strong event, caused little response in populations of fish as compared to the previous year. A similar situation is observed for the next three El Niño events (1965-1966, 1968-1969-1970, and 1972-1973), when the Peru populations of fish decrease with respect to the previous years.

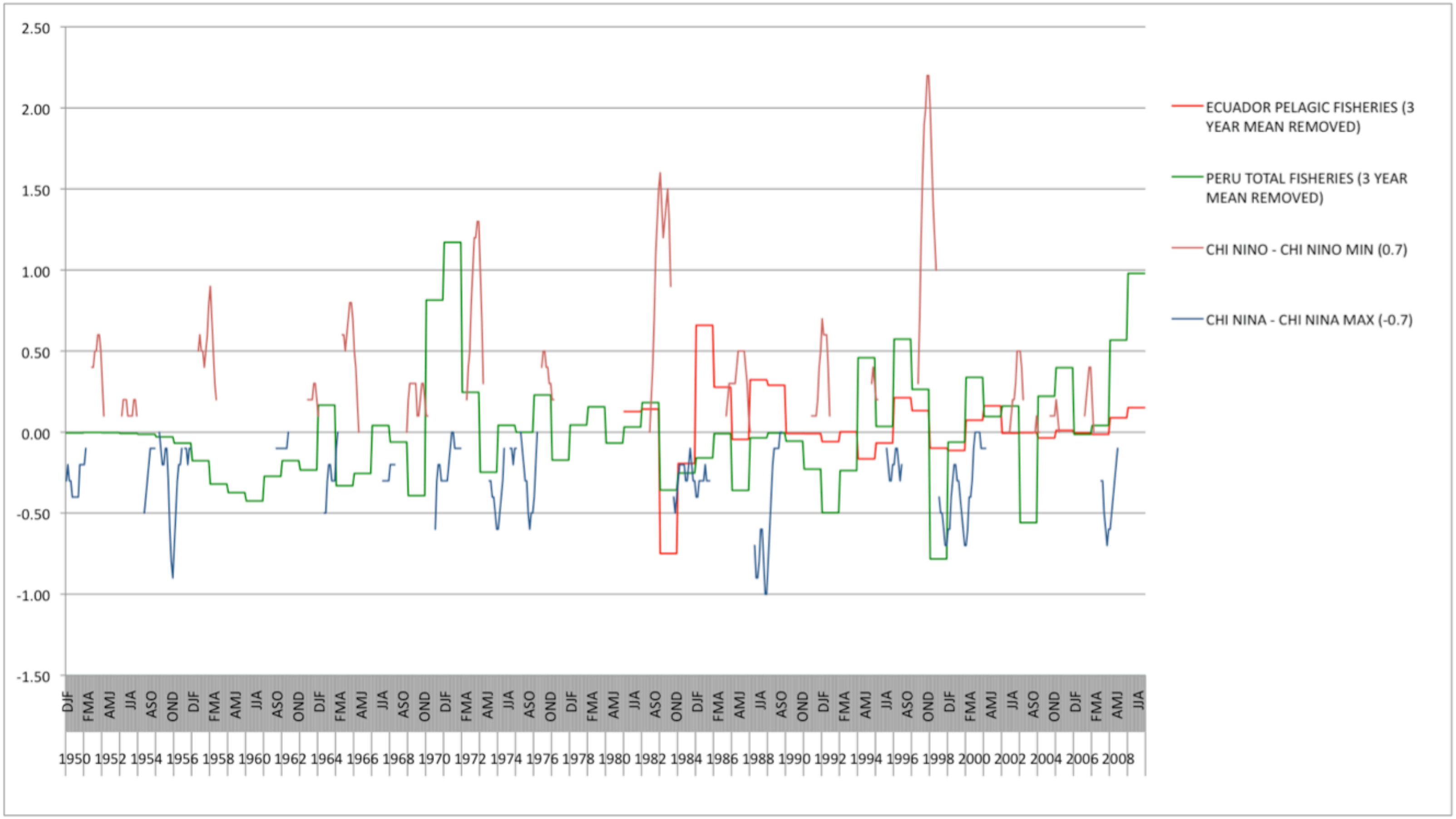

Figure 27. CHI and Ecuador and Peru Fisheries for the period 1950-2008.

The unique event in this part of the record when the population of fish increases is during the 1976-1978 El Niño event. Nonetheless, the following year (1978) the amount of fish decreases as expected. Based on the results shown in Figure 27 we find that for the first part of the analysis (1950-1981) the number of fish caught is less during El Niño events, with the exception of the El Niño of 1976-1977 when there is an offset in time between the occurrence of the warm anomalies and the decrease of the fish catch.

During the La Niña events of 1961-1962, 1964-1965, 1967-1968, and 1970-1971, the fish catch increases in Peru, as expected. Additionally, there is one La Niña event (1973-1974-1975) during which there is an offset in time between the occurrence of the cold event and the increase in fish catch, and one event (1954-1955-1956) in which the fish catch decreases during the cold event.

Analysis of the second part of the record (1981-2008) begins with a comparison between the two fisheries data sets. They show the same timing of changes either from higher to lower values and vice versa from 1981 to 1993, 1996-2003, 2006, and 2008. During 1994-1995, 2004-2005 and 2007 the fisheries data show an inverse relation. Beginning in 1981 the following El Niño events are associated with a decrease in the fish catch: 1982-1983, 1986-1987-1988, and 1997-1998. Thus, we can infer that there would be lower populations of fish with a corresponding decrease in the catch. A similar situation occurs for the El Niño events of 1991-1992 and 2002-2003, when the fish catch decreases as well, but these events occur with an offset of time with respect to the El Niño events. Finally, the cases when we observe contradictory behavior of the two fisheries data sets (Ecuador and Peru) in response to El Niño events are during the 1994-

1995 and 2006-2007 events. A special situation occurs during the El Niño event of 2004-2005. In this case both fisheries increase, opposite to what we expect in response to an El Niño event. During this latter part of the record (1981-2008) there are 5 La Niña events identified using the CHI index. The La Niña events of 1983-1984-1985 and 1988-1989 show a correspondence between cold sea surface temperature represented by CHI La Niña, and an increase in the fish catch for both countries. During the next three events there is an offset in time between the occurrence of cold SST anomalies and an increase in the fish catch.

CHAPTER IV

SUMMARY AND CONCLUSIONS

The SODA 2.2.4 ocean reanalysis is used to explore changes in upwelling from normal conditions to either El Niño or La Niña conditions. In the first part of the research we explored the physical and thermodynamic varibles in SODA 2.2.4. We used strong El Niño (CHI ≥ 1.0), and La Niña (CHI ≤ -1.0) events defined according to CHI. The region established to explore each of these variables is between 170°W and 70°W in longitude, and from 15°S to 15°N in latitude. The results obtained exploring the entrainment velocity anomaly show that the distribution of upwelling is very patchy, and we confirm that in general during El Niño years entrainment velocity decreases, and that during La Niña years entrainment velocity increases. The analysis of wind stress anomaly during El Niño years shows westerly wind anomalies, which are stronger for strong El Niño events, and during La Niña events easterlies winds are stronger due to a larger pressure gradient which agrees with ENSO theory. Consistant with previous descriptions of El Niño composite SST anomalies show a warming of 2.7 °C centered at 140°W. Zonal and meridional sections of vertical velocity were investigated as well, showing the complex distribution of changes in upwelling in the tropical Pacific during ENSO events. The results of mixed layer depth analysis show that for El Niño events in the eastern Pacific Ocean the mixed layer depth is located at 12m depth and in the western Pacific the mixed layer depth is around 104m. During La Niña events in the

eastern equatorial Pacific the mixed layer depth is located at about 5 m of depth, while in the western equatorial Pacific it deepens reaching 145m of depth.

We used three methods to compute change in upwelling during ENSO events. The first method computes upwelling within CHI areas, the second method computes the Center of Upwelling Index (CUI), and the third method computes upwelling in the Niño 1+2 region during ENSO events. The methodology applied in the three methods is similar, however the areas and conditions used in each case to calculate the parameters are different.

Using the first method we computed the upwelling in CHI areas. Upwelling changes are computed using entrainment velocity anomalies. The entrainment velocity amplitude during El Niño years shows prominent decadal variability during the entire record (1871-2008). Higher peaks in amplitude occur in the early part and the last part of the record while the middle part of the record shows low variability. This is in general agreement with the results of *Giese and Ray* [2011], who show similar behaviour for SST. For La Niña there is also decadal variability in the record, although it is not as strong as during El Niño. Using this method we also determined that during El Niño stronger negative entrainment velocity anomalies are located between 160°W and 140°W, whereas during La Niña events the anomalies occur over a wider range from 180°W to 110°W. The results show that the Center of Heat Index (CHI) and the entrainment velocity anomalies amplitudes are not strongly correlated, with a correlation of just 0.13 for El Niño events, and during La Niña events a correlation of 0.19, suggesting that upwelling does not explain much of the variance in SST. The

comparison of the time series of CHI amplitude and entrainment velocity anomaly amplitude show that the amplitude of SST anomalies during El Niño events does not have a direct relationship to changes in the rate of upwelling. During La Niña events there is no obvious relationship between peaks of the amplitude of the upwelling and peaks of SST anomalies, however the four major peaks of upwelling match four strong La Niña events. We also determine that SST anomalies are displaced eastward of the centers of upwelling during ENSO events.

The second method is to use a new Center of Upwelling Index (CUI) to compute changes in upwelling within the CUI areas. The results show that the CUI amplitude during periods of reduced upwelling has high variability with peak values in the early and the last part of the record. There is less variability in the amplitude of CUI during periods of strong upwelling. The centers of upwelling are located between 180W and 150W for both warm and cold states. We also verified that negative entrainment velocity anomalies for the early and last part of the record are east of anomalies in the middle part of the record. The analysis of positive entrainment velocity anomalies shows that there is a higher occurrence of CUI index in the last part of the record. The results obtained with this method show a weak correlation between the CHI amplitude and CUI amplitude of 0.09 for El Niño, and a correlation of 0.23 for La Niña. We emphasize that despite the fact that both indices are computed independently the timing of the amplitudes agrees very well and it is clear that the change in the rate of upwelling contributes to SST anomalies for both El Niño and La Niña events. However, strong El Niño or La Niña events do not have a direct relationship with changes in upwelling. Other processes such

as zonal advection, or heat fluxes need to be considered to explain the strength of warm and cold events. The distribution of CUI longitudes is more compact than for CHI, ranging over the central Pacific from 180°E to 155°W, and the centers of upwelling are generally west of the centers of temperature. Additionally, with this method we determine that CHI areas are much larger than the CUI areas for both El Niño and La Niña events.

We calculate upwelling changes within the Niño 1+2 region during ENSO events using two additional techniques. For the first technique the occurrence of CHI index is used, such that for every occurrence of a CHI event, upwelling is calculated. The second technique considers only the occurrence of El Niño or La Niña events located in the Eastern Pacific Ocean to identify the changes in upwelling.

Applying the first technique we determine that during El Niño events the amplitude of negative entrainment velocity anomalies has low variability for most of the record, while for La Niña the amplitude has greater variability. In addition, there is a slight tendency for strong upwelling events to occur in the period from 1960 until 2000. The results of the correlation between the Center of Heat Index and Entrainment velocity in the Niño1+2 region show a weak correlation of just 0.023 for El Niño, and a correlation of 0.0053 for La Niña. The low correlation might be due to the fact that we compare ENSO events that occur over the whole tropical Pacific Ocean with changes in upwelling over a relatively small region in the eastern Pacific. The results obtained comparing the time series of CHI amplitude and the amplitude of upwelling in the Niño

1+2 region, show that for El Niño and La Niña events only during 1960 to 1980 do the time series agree very well, while for the rest of the record there is almost no correlation.

Using the second technique to determine changes of upwelling in the Niño 1+2 region for El Niño or La Niña events located in the eastern Pacific Ocean we determine that during El Niño events the distribution of amplitude has moderate variability, while for La Niña case there is less variability.

We anticipated a high correlation between the Center of Heat Index east and Entrainment velocity in the Niño1+2 region, since we select only El Niño events that occur in the eastern Pacific. However for El Niño events the correlation is just 0.024, and for La Niña events there is no correlation. Analyzing the amplitude time series for CHI east and upwelling in the Niño 1+2 region we verified that these amplitudes agree only for the years from 1958 to 1982. From 1958 onward there are El Niño events that are prominently in the eastern Pacific (1957-1958, 1969-1970, 1972-1973, 1982-1983, and 1997-1998). Interestingly the 1969 El Niño has a strong upwelling anomaly but relatively little SST warming. The La Niña CHI east amplitude and amplitude of upwelling agree very well during three specific years (1889-1890, 1917-1918, and 1988-1989) that correspond to three strong La Niña events.

We also investigated the impact of ENSO events on the fisheries industry of Ecuador and Peru that are affected by changes in the Niño 1+2 region. The results of this comparison showed that from 1950 to 1981 the Peru fisheries data and CHI amplitude agree well. We show that during El Niño events there is a decrease in fish population, with the exception of the El Niño of 1976-1977 when there is an offset in

time between the occurrence of the warm anomalies and a decrease of the fish catch. During the La Niña events of 1961-1962, 1964-1965, 1967-1968, and 1970-1971, the fish catch increases in Peru, as expected. Additionally, there is one La Niña event (1973-1974-1975) in which there is an offset in time between the occurrence of the cold event and an increase in fish catch, and one event in which the fish catch decreases, opposite to what was expected.

The analysis of the second part of record (1981-2008), shows that the El Niño events of 1982-1983, 1986-1987-1988, and 1997-1998 are associated with a decrease in the fish catch. Thus, we infer that there were lower populations of fish with a corresponding decrease in the catch. A similar situation occurs for the El Niño events 1991-1992 and 2002-2003, when the fish catch decreases as well, but these events occur with an offset of time with respect to the El Niño events. Finally, there is contradictory behavior of the two fisheries data sets (Ecuador and Peru) in response to El Niño events are during the 1994-1995 and 2006-2007 events. A special situation occurs during the El Niño event 2004-2005. In this case both fisheries increase, opposite to what was expected in response to an El Niño event.

During the period from 1981 to 2008 there are 5 La Niña events determined using the CHI index. The La Niña events of 1983-1984-1985 and 1988-1989 show a correspondence between cold sea surface temperature represented by CHI La Niña and an increase in the fish catch for both countries. During the next three events there is an offset in time between the occurrence of cold SST anomalies and an increase in the fish catch.

REFERENCES

Anderson, J. L., B. Wyman, S. Zhang, and T. Hoar (2005), Assimilation of surface pressure observations using an ensemble filter in an idealized global atmospheric prediction system, *J. Atmos. Sci*., *62*, 2925–2938.

Battisti, D. S., and A. C. Hirst (1989), Interannual variability in the tropical atmosphere-ocean model: Influence of the basic state, ocean geometry and nonlineary, *J. Atmos. Sci*., *45*, 1687-1712.

Bloom, S. C., L. L. Takacs, A. M. da Silva, and D. Ledvina (1996), Data assimilation using incremental analysis updates, *Mon. Weather Rev*., *124*, 1256-1271, doi:10.1175/1520-0493(1996)124<1256:DAUIAU>2.0.CO;2.

Boyer, T. P., J. I. Antonov, O. K. Baranova, H. E. Garcia, D. R. Johnson, R. A. Locarnini, A. V. Mishonov, T. D. O'Brien, D. Seidov, I. V. Smolyar, and M. M. Zweng (2009), *World Ocean Database 2009*, *NOAA Atlas NESDIS*, vol. 66, edited by S. Levitus, 216 pp., DVDs, U.S. Govt. Print. Off., Washington, D. C.

Carton, J. A., and B. S. Giese (2008), A reanalysis of ocean climate using simple ocean data assimilation (SODA), *Mon. Weather Rev*., *136*, 2999-3017, doi:10.1175/2007MWR1978.1.

Compo, G. P., J. S., Whitaker, and P. D. Sardeshmukh (2006), Feasibility of a 100-year reanalysis using only surface pressure data, *Bull. Am. Meteorol. Soc*., *87*, 175-190, doi:10.1175/BAMS-87-2-175.

Compo, G. P., J. S., Whitaker, and P. D. Sardeshmukh (2008), The 20th century reanalysis project, paper presented at Third WCRP International Conference on Reanalysis, Univ. of Tokyo, Tokyo, 28 Jan. to 1 Feb. (Available at http://wcrp.ipsl.jussieu.fr/Workshops/Reanalysis2008/Documents/V5-511_ea.pdf).

Giese, B.S., and S. Ray (2011), El Niño variability in simple ocean data assimilation (SODA), 1871-2008, *J. Geophys. Res.*, *116*, C02024, doi:10.1029/2010JC006695.

Giese, B. S., G. P. Compo, N. C. Slowey, P. D. Sardeshmukh, J. A. Carton, S. Ray, and J. S. Whitaker (2010), The 1918/1919 El Niño, *Bull. Am. Meteorol. Soc., 91*, 177-183, doi:10.1175/2009BAMS2903.1.

Jin, F. -F. (1997), An equatorial ocean recharge paradigm for ENSO. Part I: Conceptual model, *J. Atmos. Sci*., *54*, 811-829.

Jones, P. W. (1999), First and second order conservative remapping schemes for grids in spherical coordinates, *Mon. Weather Rev.*, *127*, 2204-2210, doi:10.1175/1520-0493(1999)127<2204:FASOCR>2.0.CO;2.

Levitus, S., J. I. Antonov, T. P. Boyer, T. A. Locarnini, H. E. Garcia, and A. V. Mishonov (2009), Global ocean heat content 1955-2008 in light of recently revealed instrumentation problems, *Geophys. Res. Lett.*, *36*, L07608, doi:10.1029/2008GL037155.

Philander, S. G. (1990), *El Niño, La Niña, and the Southern Oscillation*, 289pp., Academic Press, London.

Picaut, J., F. Masia, and Y. du Penhoat (1997), An advective-reflective conceptual model for the oscillatory nature of the ENSO, *Science*, *274*, 1486-1489.

Sarachik E. S., and M. A. Cane (2010), *The El Niño Southern Oscillation Phenomenon*, 369pp., University Press, Cambridge, 369pp.

Smith, R. D., J. K. Dukowicz, and R. C. Malone (1992), Parallel ocean general circulation modeling, *Physica D*, *60*, 38-61, doi:10.1016/0167-2789(92)90225-C.

Suarez, M. J., and P. S. Schopf (1988), A delayed action oscillator for ENSO, *J. Atmos. Sci*., *45*, 3283-3287.

Walker, G. T. (1923), Correlation in seasonal variations of weather. VIII. A preliminary study of world weather, *Mem. Indian Meteorol. Dep*., *24*, 75-131.

Walker, G. T. (1924), Correlation in seasonal variations of weather. IX. A further study of world weather, *Mem. Indian Meteorol. Dep*., *24*, 275-332.

Walker, G. T., and E. W. Bliss (1932), World weather, V. *Mem. R. Meteorol. Soc*., *4*, 53-84.

Wang, C. (2001), A unified oscillator model for the El Niño-Southern Oscillation, *J. Clim*., *14*, 98-115.

Wang, C., R. H. Weisberg, and H. Yang (1999), Effects of the wind speed-evaporation-SST feedback on the El Niño-Southern Oscillation, *J. Atmos. Sci*., *56*, 1391-1403.

Wang, C. and P. Fiedler (2006), ENSO variability and the Eastern Tropical Pacific: A review, *Prog. in Oceanog.*, *69*, 239-266, doi:10.1016/j.pocean.2006.03.004.

Wang, C. and J. Picaut (2004), Understanding ENSO Physics-A review, In: Wang, C., Xie, S. P., Carton, J. (Eds), Earth's Climate: The Ocean-Atmosphere Interaction, *Geophysical Monograph Series*, *147*, 21-48, doi:10.1029/147GM02.

Weisberg, R. H., and C. Wang (1997), A western Pacific oscillator paradigm for the El Niño-Southern Oscillation, *Geophys. Res. Lett*., *24*, 779-782, doi:10.1029/97GL00689.

Whitacker, J. S., and T. M. Hamill (2002), Ensemble data assimilation without perturbed observations, *Mon. Weather Rev.*, *130*, 1913-1924, doi:10.1175/1520-0493(2002)130<1913:EDAWPO>2.0.CO;2.

Whitacker, J. S., G. P. Compo, X. Wei, and T. M. Hamill (2004), Reanalysis without radiosondes using ensemble data assimilation, *Mon. Weather Rev*., *132*, 1190-1200, doi:10.1175/1520-0493(2004)132<1190:RWRUED>2.0.CO;2.

VITA

Name:	Carlos Fernando Perugachi Salamea
Address:	Instituto Oceanográfico de la Armada, Base Naval Sur, Guayaquil, Ecuador
Email Address:	cperugachis@tamu.edu
Education:	B.S., Naval Sciences, America Technological University, 2003.